Sterile Neutrinos and Non-Standard Interactions in Neutrino Telescopes

Martin Sjöborg

Particle and Astroparticle Physics, Department of Physics
Royal Institute of Technology, SE-106 91 Stockholm, Sweden

Stockholm, Sweden 2021

Examensarbete för avläggande av masterexamen i Teknisk fysik, inom ämnesområdet teoretisk fysik.
Master’s thesis for the degree of Master of Science, in the subject area of Theoretical Physics.

TRITA-SCI-GRU 2021:042

Abstract

Lorem ipsum dolor sit amet, consectetuer adipiscing elit. Ut purus elit, vestibulum ut, placerat ac, adipiscing vitae, felis. Curabitur dictum gravida mauris. Nam arcu libero, nonummy eget, consectetuer id, vulputate a, magna. Donec vehicula augue eu neque. Pellentesque habitant morbi tristique senectus et netus et malesuada fames ac turpis egestas. Mauris ut leo. Cras viverra metus rhoncus sem. Nulla et lectus vestibulum urna fringilla ultrices. Phasellus eu tellus sit amet tortor gravida placerat. Integer sapien est, iaculis in, pretium quis, viverra ac, nunc. Praesent eget sem vel leo ultrices bibendum. Aenean faucibus. Morbi dolor nulla, malesuada eu, pulvinar at, mollis ac, nulla. Curabitur auctor semper nulla. Donec varius orci eget risus. Duis nibh mi, congue eu, accumsan eleifend, sagittis quis, diam. Duis eget orci sit amet orci dignissim rutrum.

Sammanfattning

Lorem ipsum dolor sit amet, consectetuer adipiscing elit. Ut purus elit, vestibulum ut, placerat ac, adipiscing vitae, felis. Curabitur dictum gravida mauris. Nam arcu libero, nonummy eget, consectetuer id, vulputate a, magna. Donec vehicula augue eu neque. Pellentesque habitant morbi tristique senectus et netus et malesuada fames ac turpis egestas. Mauris ut leo. Cras viverra metus rhoncus sem. Nulla et lectus vestibulum urna fringilla ultrices. Phasellus eu tellus sit amet tortor gravida placerat. Integer sapien est, iaculis in, pretium quis, viverra ac, nunc. Praesent eget sem vel leo ultrices bibendum. Aenean faucibus. Morbi dolor nulla, malesuada eu, pulvinar at, mollis ac, nulla. Curabitur auctor semper nulla. Donec varius orci eget risus. Duis nibh mi, congue eu, accumsan eleifend, sagittis quis, diam. Duis eget orci sit amet orci dignissim rutrum.

Acknowledgements

The computations were enabled by resources provided by the Swedish National Infrastructure for Computing (SNIC) at HPC2N, Umeå University and NSC, Linköping University. The resources were partially funded by the Swedish Research Council through grant agreement no. 2018-05973

Contents

Chapter 1

Introduction

There is no reason for us to believe that our current knowledge in particle physics is complete. The most successful framework – the Standard Model – has notable shortcomings. Neither does it explain why there is something rather than nothing, nor does it give a candidate for dark matter[1]. To make matters even worse, three of the massless particles have been observed to have mass. In this thesis, we focus on the said particles – the neutrinos – and propose extensions to the Standard Model related to them. We then compare the effects of these extensions with collected data to see if our new theory more closely describes Nature or not.

Ultimately, the purpose of this excursion is to guide future research where to uncover more accurate theories. Traces of this grander theory will be present as breadcrumbs scattered in Nature. We just need to know where and how carefully to look.

1.1 Outline

This thesis is outlined as follows. In Chapter 2, we briefly review the most relevant parts of the Standard Model that will be relevant for our extensions of it. Then we present the evidence and subsequent discovery of neutrino oscillations, which ultimately led to the 2015 Nobel physics prize, along with the modifications to the Standard Model needed to accommodate the discovery. The reader is then introduced to a standard but detailed derivation of the neutrino mixing matrix and oscillation Hamiltonian, including the matter effects stemming from charged and neutral current weak interactions within the Earth.

In Chapter 3, we present an experimental procedure used to observe signals from neutrinos originating from cosmic ray interactions in the atmosphere of the Earth. Furthermore, present the two present Antarctic neutrino detectors: IceCube and DeepCore. We also summarize a proposed detector upgrade: Precision IceCube Next Generation Upgrade (PINGU), which we will use as a forecast in our analysis.

Chapter 4 consists of two parts. In Section 4.1, we introduce a new particle: the sterile neutrino. We present how neutrino oscillations are modified by this hypothesized fourth neutrino and how these modifications would appear in IceCube if the particle is present in Nature. In Section 4.2, we completely set the sterile neutrino aside and instead turn to the interactions between neutrinos and the Earth. We again amend the Standard Model by considering exotic interactions from a higher energy theory, manifesting themselves as sub-leading modifications to the matter potential. Since these new interactions are not present in the Standard Model, we call them non-standard interactions (NSI).

Finally, Chapter 5 contains the result from our two separate extensions of the Standard Model. In Section 5.1 we present our findings for the sterile neutrino and compare those with literature. In Section 5.2, we present new constrained bounds on the NSI parameters by combining our results for IceCube, DeepCore, and PINGU.

[1] In the Standard Model, matter and antimatter come in pairs of one particle and one antiparticle. When interacting, antimatter *annihilates* the matter, resulting in pure light. Since the universe exists, there must have been more matter than antimatter at the Big Bang. This baryon asymmetry is unexplained in the Standard Model. Dark matter is heavy matter which does not interact with electromagnetic radiation. No such particle exists in the Standard Model.

Chapter 2

Neutrino Oscillations

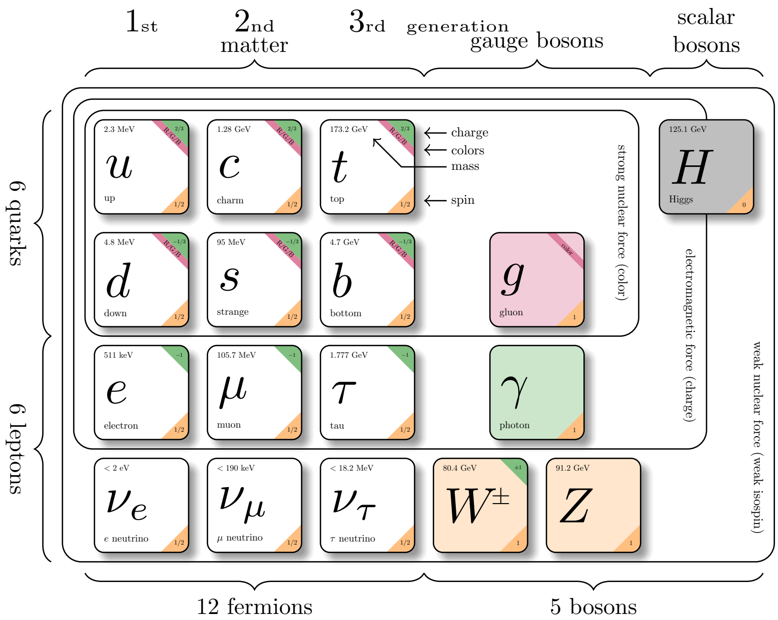

2.1 The Standard Model

In order to describe the three quantizable forces of nature, we gather the mediators of each force – the vector bosons – into local (gauge) symmetry groups. Each vector boson has one corresponding generator, the set of which constitutes the group. The strong charge is mediated by eight massless gluons, which correspond to the eight generators of $\mathrm{SU}(3)_C$. The weak charge is mediated by the three massive gauge bosons $W^{\pm}$ and Z, and the massless photon γ, which constitute the generators of $\mathrm{SU}(2)_L$ and $\mathrm{U}(1)_Y$.

The subscript of each group denotes by which mechanism that force is mediated. The gluons mediate the strong force through interactions of color, emphasized with subscript C. The weak force only sees left-handed particles, which we distinguish with the subscript L. And the electroweak interaction that a particle undergoes is determined by its hypercharge Y. For example, the quarks all have a nonzero color and hypercharge, so they participate in the strong and electromagnetic interactions. If a quark is left-handed, it will also feel the weak interaction. The neutrinos on the other hand, have neither charge nor color, so they are insivible to both the strong and electromagnetic force. We express this by letting their fields transform as singlets under those symmetry groups.

Together, these three interactions make up the Standard Model gauge group $\mathrm{SU}(3)_\mathrm{C} \times \mathrm{SU}(2)_L \times \mathrm{U}(1)_Y$. This determines the form of the three coupling constants, but which numerical values must be experimentally measured. Since the vector bosons are represented by the generators, they are uniquely determined by the symmetry group. However, the scalar boson(s) and fermions are free as long as they belong to representations of the symmetry group. By this construction, the fermions have more degrees of freedom with which we can propose amendments to the model with. Even the number of fermions must be experimentally verified and can be altered from a phenomenological standpoint. In this work, we will use this leniency to make drastic modifications to the Standard Model fermions and examine to which extent these modifications might be supported by experimental evidence.

2.2 Neutrino Mixing

In 1998, the Super-Kamiokande collaboration detected a ν_μ deficit that could not be explained by any other mechanism than the conversion of muon neutrinos to electron neutrinos. This was the first conclusive evidence of a $\nu_\mu \to \nu_e$ oscillation. The most interesting conclusion from the observation of neutrino flavor oscillations is the equivalence between oscillations and neutrino mass, with the latter being identically zero acording to the Standard Model. Thus, we are required to extend the Standard Model to incorporate neutrino masses before we discuss the neutrino oscillations themselves.

2.2.1 Mass Generation

In the Standard Model, fermion masses are generated by the Higgs mechanism through Yukawa couplings with the fermion's right and left-handed components. All neutrinos are left-handed and all antineutrinos are right-handed. Thus, neutrinos are massless since they do not undergo the Higgs mechanism. Additionally, all terms of a Lagrangian that we construct must respect the gauge invariance. This removes the possibility of the neutrino mass to be generated at loop level because any such attempt will violate the total lepton number by two units. In order to keep our theory renormalizable, we have one option left if we want to generate neutrino masses: introducing additional fermions.

We consider a right-handed neutrino field, ν_R. Since the electroweak gauge group $\mathrm{SU}(2)_L \times U(1)_Y$ only couple to left-handed particles and right-handed antiparticles, ν_R transforms as a singlet under the Standard Model symmetry group $\mathrm{SU}(3)_C \times \mathrm{SU}(2)_L \times \mathrm{U}(1)_Y$. This neutrino field is *sterile* since it doesn't participate any of the Standard Model interactions.

We extend the Standard Model by adding a right-handed component of this field with neutrino Yukawa couplings $Y'^{\nu}_{\alpha\beta}$ to the Higgs-lepton Yukawa Lagrangian

$$\mathcal{L}_H = -\left(\frac{v+H}{\sqrt{2}}\right)\left[\ell'_{\alpha L} Y'^{\ell}_{\alpha\beta} \ell'_{\beta R} + \nu'_{\alpha L} Y'^{\nu}_{\alpha\beta} \nu'_{\beta R}\right] . \tag{2.1}$$

Now, the Yukawa coupling matrices Y'^{ℓ} and Y'^{ν} are non-diagonal, with the former resulting in the charged lepton masses being non-definite. This can be remedied by diagonalizing Y'^{ℓ} with a unitary matrix V^{ℓ} as

$$V^{\nu\dagger}_{\alpha k L} Y'^{\nu}_{\alpha\beta} V^{\nu}_{\beta j R} = Y^{\nu}_{kj} . \tag{2.2}$$

Similarily, we diagonalize and Y'^{ν} with a unitary matrix V^{ν}. We note that this will not yet generate neutrino masses, since no flavor rotation can make massless fields massive. Now we state a crucial difference between the properties of the charged lepton and the neutrino fields. While the charged lepton flavor eigenstate was uniquely determined by its mass eigenstate, the neutrino flavor is a superposition of mass eigenstates. This is because neutrinos are indirectly detected via the observation of its associated charged lepton, so there is no requirement of neutrino flavor eigenstates to have a definite mass. The flavor of a neutrino is then, by definition, the flavor of the associated charged lepton. This fact is introduced as giving the mass eigenstates Latin numerals and letters, while the flavor eigenstates stay as Greek letters.

So, let the neutrino field with chriality X be denoted ν_X, with components having Latin numerals to distinguish them from the flavour components, i.e

$$\nu_{kX} = V^{\nu\dagger}_{k\beta X} \nu'_{\beta X} . \tag{2.3}$$

The diagonalized Lagrangian now takes the form

$$\begin{aligned}
\mathcal{L}_H &= -\left(\frac{v+H}{\sqrt{2}}\right)\left[\ell'_{\alpha L} Y'^{\ell}_{\alpha\beta} \ell'_{\beta R} + \nu'_{\alpha L} Y'^{\nu}_{\alpha\beta} \nu'_{\beta R}\right] \\
&= -\left(\frac{v+H}{\sqrt{2}}\right)\left[\ell'_{\alpha L} V^{\ell}_{\alpha\beta L} Y^{\ell}_{\alpha\beta} V^{\ell\dagger}_{\alpha\beta R} \ell'_{\beta R} + \nu'_{\alpha L} V^{\nu}_{\alpha k L} Y^{\nu}_{kj} V^{\nu\dagger}_{\beta j R} \nu'_{\beta R}\right] \\
&= -\left(\frac{v+H}{\sqrt{2}}\right)\left[\ell^{\dagger}_{\alpha L} Y^{\ell}_{\alpha\beta} \ell_{\beta R} + \nu^{\dagger}_{kL} Y^{\nu}_{kj} \nu_{jR}\right] \\
&= -\left(\frac{v+H}{\sqrt{2}}\right)\left[\bar{\ell}_{\alpha L} Y^{\ell}_{\alpha\beta} \ell_{\beta R} + \bar{\nu}_{kL} Y^{\nu}_{kj} \nu_{jR}\right]
\end{aligned} \tag{2.4}$$

By construction, Y^ℓ and Y^ν are diagonal, so we write their omponents as $y^\ell_\alpha \delta_{\alpha\beta}$ and $y^\nu_k \delta_{kj}$ respectively, leaving the Lagrangian as

$$\begin{aligned}\mathcal{L}_H &= -\left(\frac{v+H}{\sqrt{2}}\right)\left[\bar{\ell}_{\alpha L} y^\ell_\alpha \delta_{\alpha\beta} \ell_{\beta R} + \bar{\nu}_{kL} y^\nu_k \delta_{kj} \nu_{jR}\right] \\ &= -\left(\frac{v+H}{\sqrt{2}}\right)\left[\bar{\ell}_{\alpha L} y^\ell_\alpha \ell_{\alpha R} + \bar{\nu}_{kL} y^\nu_k \nu_{kR}\right] \\ &= -\left(\frac{v+H}{\sqrt{2}}\right)\left[y^\ell_\alpha \bar{\ell}_{\alpha L} \ell_{\alpha R} + y^\nu_k \bar{\nu}_{kL} \nu_{kR}\right] \end{aligned} \tag{2.5}$$

Now, by the introduction of the sterile field ν_R, the Dirac neutrino field is

$$\nu_k = \nu_{kL} + \nu_{kR}\,. \tag{2.6}$$

Multiplying ν_k with its conjugate $\bar{\nu}_k$, we get

$$\begin{aligned}\bar{\nu}_k \nu_k &= \bar{\nu}_{kL}\nu_{kL} + \bar{\nu}_{kR}\nu_{kL} + \bar{\nu}_{kL}\nu_{kR} + \bar{\nu}_{kR}\nu_{kR} \\ &= \bar{\nu}_{kL}\nu_{kR} + \bar{\nu}_{kR}\nu_{kL} \\ &= \bar{\nu}_{kL}\nu_{kR} + \text{h.c.}\end{aligned} \tag{2.7}$$

The same calculation for the charged lepton field yields the same result for ℓ_k. Substituting this result and expanding the Higgs vacuum expectation value v into the fields gives us

$$\begin{aligned}\mathcal{L}_H &= -\left(\frac{v+H}{\sqrt{2}}\right)\left[y^\ell_\alpha \bar{\ell}_\alpha \ell_\alpha + y^\nu_k \bar{\nu}_k \nu_k\right] \\ &= -\frac{y^\ell_\alpha v}{\sqrt{2}}\bar{\ell}_\alpha \ell_\alpha - \frac{y^\nu_k v}{\sqrt{2}}\bar{\nu}_k \nu_k - \frac{y^\ell_\alpha}{\sqrt{2}}\bar{\ell}_\alpha \ell_\alpha H - \frac{y^\nu_k}{\sqrt{2}}\bar{\nu}_k \nu_k H\,.\end{aligned} \tag{2.8}$$

Thus, this extension to the SM generates by the Higgs mechanism neutrino masses with terms

$$m_k = \frac{y^\nu_k v}{\sqrt{2}}\,, \tag{2.9}$$

where the Yukawa couplings y^ν_k needs to be experimentally determined.

2.2.2 The Mixing Matrix

Substituting the new transformation from Eq. 2.3 into the expression for the weak charged current, we get

$$\begin{aligned}j^\rho_L &= 2\bar{\nu}'_{\alpha L}\gamma^\rho \ell'_{\alpha L} \\ &= 2\bar{\nu}_{kL} V'^{\nu\dagger}_{k\alpha} V'^{\ell}_{\alpha\alpha}\gamma^\rho \ell_{\alpha L}\end{aligned} \tag{2.10}$$

Now, the current in Eq. 2.10 conserves lepton number, since the neutrino field with flavor α only couples to the lepton field with flavor α. Thus, neutrino interactions still conserve lepton number. However, the Higgs-lepton Yukawa Lagrangian in Eq. 2.5 violates lepton number conservation since it couples the charged lepton flavor α to the neutrino mass eigenstate k, which is a superposition of flavors. There is no transformation that leaves both the interaction and kinetic Lagrangian invariant, thus violating this symmetry.

Call $V'^{\nu\dagger}_{k\alpha} V'^{\ell}_{\alpha\alpha} = U^\dagger_{k\alpha}$. We will refer to the matrix U built by the components $U_{k\alpha}$ as the Pontecorvo-Maki-Nakagawa-Sakata (PMNS) matrix [1, 2]. We now have

$$j^\rho_L = 2\sum_\alpha \sum_k U^\dagger_{\alpha k}\bar{\nu}_{kL}\gamma^\rho \ell_{\alpha L}\,. \tag{2.11}$$

What form does this new matrix U take? By construction, it provides the unitary transformation between the flavor and mass bases. Any unitary 3×3 matrix can be parametrized using three mixing angles and six phases. However, not all phases affect the charged and weak currents and are thus not observable. Moreover, both the Lagrangian and the currents are invariant under global $U(1)$ transformations, leaving only one physical phase for us to measure. Thus we are down to four degrees of freedom in the three dimensional case: three mixing angles of the form $\sin(\theta_{ij})/\cos(\theta_{ij}) = s_{ij}/c_{ij}$, and one phase of the form $e^{i\delta}$.

We construct the PMNS matrix using the rotation matrixes from $SO(3)$ as

$$\begin{aligned} U &= R_{23}R_{13,\delta_{\mathrm{CP}}}R_{12} \\ &= \begin{pmatrix} 1 & 0 & 0 \\ 0 & c_{23} & s_{23} \\ 0 & -s_{23} & c_{23} \end{pmatrix} \begin{pmatrix} c_{13} & 0 & s_{13}e^{-i\delta_{\mathrm{CP}}} \\ 0 & 1 & 0 \\ -s_{13}e^{i\delta_{\mathrm{CP}}} & 0 & c_{13} \end{pmatrix} \begin{pmatrix} c_{12} & s_{12} & 0 \\ -s_{12} & c_{12} & 0 \\ 0 & 0 & 1 \end{pmatrix} . \end{aligned} \tag{2.12}$$

The term δ_{CP} determines the degree of charge-parity violation. In this work, we will assume CP invariance by always setting $\delta_{CP} = 0°$. Thus,

$$\begin{aligned} U &= \begin{pmatrix} 1 & 0 & 0 \\ 0 & c_{23} & s_{23} \\ 0 & -s_{23} & c_{23} \end{pmatrix} \begin{pmatrix} c_{13} & 0 & s_{13} \\ 0 & 1 & 0 \\ -s_{13} & 0 & c_{13} \end{pmatrix} \begin{pmatrix} c_{12} & s_{12} & 0 \\ -s_{12} & c_{12} & 0 \\ 0 & 0 & 1 \end{pmatrix} \\ &= \begin{pmatrix} c_{12}c_{13} & s_{12}c_{13} & s_{13} \\ -s_{12}c_{23} - c_{12}s_{23}s_{13} & c_{12}c_{23} - s_{12}s_{23}s_{13} & s_{23}c_{13} \\ s_{12}s_{23} - c_{12}c_{23}s_{13} & -c_{12}s_{23} - s_{12}c_{23}s_{13} & c_{23}c_{13} \end{pmatrix} . \end{aligned} \tag{2.13}$$

In this work, we will be using the best-fit values from [3] with the exception of the CP-violating phase δ_{CP}. The 90% CL values are

$$\theta_{12} = 33.44°, \quad \theta_{13} = 8.57°, \quad \theta_{23} = 49.2°, \quad \delta_{\mathrm{CP}} = 0\,. \tag{2.14}$$

The PMNS matrix is then real, with numerical values

$$U = \begin{pmatrix} U_{e1} & U_{e2} & U_{e3} \\ U_{\mu 1} & U_{\mu 2} & U_{\mu 3} \\ U_{\tau 1} & U_{\tau 2} & U_{\tau 3} \end{pmatrix} = \begin{pmatrix} 0.825 & 0.545 & 0.149 \\ -0.455 & 0.485 & 0.746 \\ 0.334 & -0.684 & 0.649 \end{pmatrix} . \tag{2.15}$$

In our study, we will only use neutrinos originating from conventional cosmic ray interactions in the atmosphere. In this so-called atmospheric neutrino flux, ν_μ are the most abundant, while the ν_τ flux is neglible. We see that $U_{\mu\tau}$ is the largest $U_{\mu\beta}$ term, suggesting that ν_μ primarily mixes into ν_τ, at least in vacuum. It turns out that matter effects indeed preserves this ordering, making the $\nu_\mu \to \nu_\tau$ transition the most abundant. This means we will be able to stringently constrain parameters relating to $\mu\tau$ mixing.

2.2.3 Neutrino Propagation

Since we now know how the neutrino mass and flavor eigenstates combine, and have an expression for the flavor interaction with the neutrino's charged lepton partner, we are now ready to study the flavor oscillations themselves.

Now, the Fourier expansion of the field operator $\bar{\nu}_{kL}$ in the current of Eq. 2.11 contains creation operators $a^\dagger_{\nu_k}$ of massive neutrinos with mass m_k. This means that the summation over the mass index k constructs a flavor neutrino, which interacts with the charged lepton field $\ell_{\alpha L}$. In other words, the charged current generates a flavor neutrino ν_α, which is a superposition of the mass eigenstates ν_k with weights $U^\dagger_{\alpha k}$. In the ket-formalism, we express this as

$$|\nu_\alpha\rangle = \sum_k U^\dagger_{\alpha k} |\nu_k\rangle \ . \tag{2.16}$$

It is the mass eigenstates $|\nu_k\rangle$ that are eigenstates of the Hamiltonian, with eigenvalues

$$E_k = \sqrt{\vec{p}^2 + m_k^2}\,. \tag{2.17}$$

The solution to the time-dependent Schrödinger equation

$$i\frac{\mathrm{d}}{\mathrm{d}t} |\nu_k(t)\rangle = H_0 |\nu_k(t)\rangle \ , \tag{2.18}$$

where H_0 is the Hamiltonian and the subscript signifies that we are in vacuum.

The solution to Eq. 2.18 gives ut the time evolution in the form of plane wave solutions:

$$|\nu_k(t)\rangle = e^{-iE_k t} |\nu_k\rangle \ . \tag{2.19}$$

Inserting the plane wave solution into Eq. 2.16, we get

$$|\nu_\alpha(t)\rangle = \sum_k U^\dagger_{\alpha k} e^{-iE_k t} |\nu_k\rangle \ . \tag{2.20}$$

Now we know how to evolve and combine the mass eigenstates to form a flavor eigenstate, but how about the reverse? We swap the index $k \to j$ in Eq. 2.16 and multiply by $U_{\alpha k}$:

$$\begin{aligned}\sum_\alpha U_{\alpha k} |\nu_\alpha\rangle &= \sum_{\alpha,j} U_{\alpha k} U^\dagger_{\alpha j} |\nu_j\rangle \\ &= \sum_j \delta_{kj} |\nu_j\rangle \\ &= |\nu_k\rangle \ ,\end{aligned} \tag{2.21}$$

where we have used the unitarity of the leptonic mixing matrix. Eqs. 2.16 and 2.20 yield

$$\begin{aligned}|\nu_\alpha(t)\rangle &= \sum_k U^\dagger_{\alpha k} e^{-iE_k t} |\nu_k\rangle \\ &= \sum_k U^\dagger_{\alpha k} e^{-iE_k t} \left(\sum_\beta U_{\beta k} |\nu_\beta\rangle \right) \\ &= \sum_{k,\beta} U^\dagger_{\alpha k} U_{\beta k} e^{-iE_k t} |\nu_\beta\rangle \ .\end{aligned} \tag{2.22}$$

The probability of the flavor transition $\nu_\alpha \to \nu_\beta$ at time t is $|\langle \nu_\beta | \nu_\alpha(t)\rangle|^2$:

$$P_{\nu_\alpha \to \nu_\beta}(t) = \sum_{k,j} U^\dagger_{\alpha k} U_{\beta k} U^\dagger_{\beta j} U_{\alpha j} e^{-i(E_k - E_j)t} \ . \tag{2.23}$$

We assume the neutrino masses m_k to be extremely small compared to their associated energies E_k. Thus, $v \sim 1$, and $|\vec{p}| \sim E$ making the energy-dispersion relation of Eq. 2.17 to first order:

$$\begin{aligned}E_k &= \sqrt{\vec{p}^2 + m_k^2} \\ &= \vec{p}^2 \sqrt{1 + \frac{m_k^2}{\vec{p}^2}} \\ &\approx E + \frac{m_k^2}{2E}\end{aligned} \tag{2.24}$$

Hence, the exponential can be simplified, and simplifying the notation $P_{\nu_\alpha \to \nu_\beta}(t) \to P_{\alpha\beta}(t)$ we get

$$P_{\alpha\beta}(t) = \sum_{k,j} U^\dagger_{\alpha k} U_{\beta k} U^\dagger_{\beta j} U_{\alpha j} e^{-i(m_k^2 - m_j^2)t/2E} \ . \tag{2.25}$$

Now, our approximation $v \approx 1$ implies $x \approx t$, thus

$$\begin{aligned}P_{\alpha\beta}(x) &= \sum_{k,j} U^\dagger_{\alpha k} U_{\beta k} U^\dagger_{\beta j} U_{\alpha j} e^{-i(m_k^2 - m_j^2)x/2E} \\ &= \sum_{k,j} U^\dagger_{\alpha k} U_{\beta k} U^\dagger_{\beta j} U_{\alpha j} \exp\left(-i \frac{\Delta m^2_{kj} x}{2E} \right) ,\end{aligned} \tag{2.26}$$

where we in the last step have defined the *mass squared-difference* $\Delta m^2_{kj} = m_k^2 - m_j^2$. Since the oscillation probability depends on this quantity rather than the individual masses, it is impossible to measure the mass m_k through neutrino oscillations. Squaring the unitarity condition $\sum_k U_{\alpha k} U^\dagger_{\beta k} = \delta_{\alpha\beta}$ yields

$$\sum_k |U_{\alpha k}|^2 |U_{\beta k}|^2 = \delta_{\alpha\beta} - 2 \sum_{k>j} \mathrm{Re}[U^\dagger_{\alpha k} U_{\beta k} U_{\alpha j} U^\dagger_{\beta j}] \tag{2.27}$$

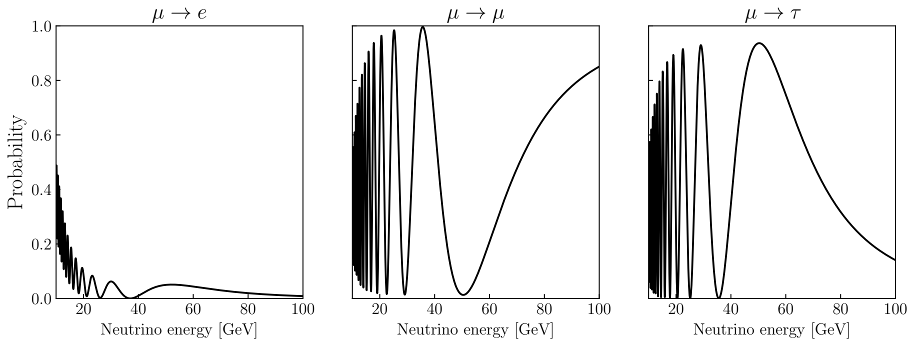

Figure 2.1: ν_μ vacuum oscillations from Eq. 2.28

Since we take the PMNS matrix to be real and thus Hermitian, we drop the complex transpose in the following calculation. We have

$$
\begin{aligned}
P_{\alpha\beta} &= \sum_{k,j} U_{\alpha k}U_{\beta k}U_{\beta j}U_{\alpha j}\exp\left(-i\frac{\Delta m_{kj}^2 x}{2E}\right) \\
&= \sum_k |U_{\alpha k}|^2|U_{\beta k}|^2 + \sum_{k\neq j} U_{\alpha k}U_{\beta k}U_{\beta j}U_{\alpha j}\exp\left(-i\frac{\Delta m_{kj}^2 x}{2E}\right) \\
&= \delta_{\alpha\beta} - 2\sum_{k>j} U_{\alpha k}U_{\beta k}U_{\beta j}U_{\alpha j} + \sum_{k\neq j} U_{\alpha k}U_{\beta k}U_{\beta j}U_{\alpha j}\exp\left(-i\frac{\Delta m_{kj}^2 x}{2E}\right) \\
&= \delta_{\alpha\beta} - 2\sum_{k>j} U_{\alpha k}U_{\beta k}U_{\beta j}U_{\alpha j} + 2\sum_{k>j} U_{\alpha k}U_{\beta k}U_{\beta j}U_{\alpha j}\exp\left(-i\frac{\Delta m_{kj}^2 x}{2E}\right) \\
&= \delta_{\alpha\beta} - 2\sum_{k>j} U_{\alpha k}U_{\beta k}U_{\beta j}U_{\alpha j}\left[1-\exp\left(-i\frac{\Delta m_{kj}^2 x}{2E}\right)\right] \\
&= \delta_{\alpha\beta} - 2\sum_{k>j} U_{\alpha k}U_{\beta k}U_{\beta j}U_{\alpha j}\sin^2\left(\frac{\Delta m_{kj}^2 x}{4E}\right), \qquad (2.28)
\end{aligned}
$$

which is the probability of neutrino vacuum oscillations. The calculation for antineutrinos yield the same result if one continues to assume the realness of the mixing matrix. In Fig. 2.1, we show the energy spectra of these oscillations in the low GeV range for neutrinos that travel 12 000 km[1]. In the left-most panel, we see a supressed $\nu_\mu \to \nu_e$ transition. We can understand this behavior by studying Eq. 2.28 and the numerical values of the mixing matrix in Eq. 2.15. GeV oscillations are driven by the Δm_{31}^2 mass-squared difference. Hence, the most important mixing matrix elements for $P_{\alpha\beta}$ are $U_{\alpha 3}, U_{\alpha 1}$ and $U_{\beta 3}, U_{\beta 1}$. The smallness of U_{e3} then supresses the amplitude of $P_{\mu e}$.

For our purposes, the probabilities in Eq. 2.28 are rather uninteresting, since they are only valid in vacuum. Despite this fact, this form elucidates an important aspect of neutrino oscillations. The mixing matrix elements determine the amplitude of the oscillations, while the mass-squared differences together with the ratio L/E determine the frequency.

2.2.4 Effective Potentials

In this work, we are concerned about the interactions with the neutrino and Earth-like matter, i.e. electrons, protons, and neutrons. The possible interactions are shown in Fig. 2.2. The left panel shows that the only flavor that can go through charged current (CC) interactions is the electron flavor. This is because the Earth doesn't consist of any muons or tau particles. The right panel shows any neutrino flavor interaction via the neutral current (NC) with Earth-like matter[2], mediated by the neutral Z boson

[1]This baseline is approximately the Earth diameter, and will be the maximum travel distance which we will use later on.

[2]The Earth is entirely composed of electrons, protons, and neutrons. Thus, the fundamental particles composing Earth are electrons, and up and down quarks. We refer to this as *Earth-like matter*.

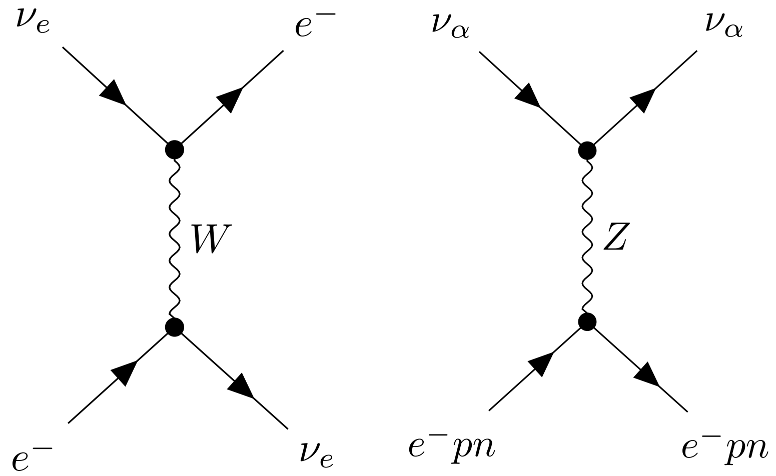

(a) Charged current weak interaction between an electron neutrino and an electron, mediated by either a W^+ or W^- boson.

(b) Neutral current weak interaction between a neutrino of any flavor and a Earth-like fermion, mediated by a neutral Z boson.

Figure 2.2: Feyman diagrams showing the two interactions that neutrinos participate in according to the Standard Model.

The interaction mediated by the W boson will give rise to a effective matter potential V_{CC}, while the Z boson is responsible for V_{NC}. Our task is now to find expressions for these.

We start with the effective Hamiltonian for the CC process. The Feynman rules for the left panel give us

$$H_{CC} = \frac{G_F}{\sqrt{2}} \left[\bar{\nu_e}\gamma^\rho \left(1-\gamma^5\right) e\right] \left[\bar{e}\, \gamma_\rho \left(1-\gamma^5\right) \nu_e\right] \tag{2.29}$$

By using the Fierz transformation

$$\mathcal{L}^{V-A}(\psi_1, \psi_2, \psi_3, \psi_4) = \mathcal{L}^{V-A}(\psi_1, \psi_4, \psi_3, \psi_2)\,, \tag{2.30}$$

we can permute the terms inside the brackets, yielding

$$H_{CC} = \frac{G_F}{\sqrt{2}} \left[\bar{\nu_e}\gamma^\rho \left(1-\gamma^5\right) \nu_e\right] \left[\bar{e}\, \gamma_\rho \left(1-\gamma^5\right) e\right] \,. \tag{2.31}$$

Now, lets consider a finite volume V with electron states defined as

$$|e(p_e, h_e)\rangle = \frac{1}{2E_e V}\, a_e^{(h_e)\dagger}(p_e)\, |0\rangle \,, \tag{2.32}$$

i.e. using the creation operator $a_e^{(h_e)\dagger}(p_e)$ to create electron states from vacuum with momenta p_e, energy E_e, and helicity h_e. The density distribution of electrons in V is $f(E_e, T)$, which we normalize to the total number of electrons as we integrate out the momenta p_e:

$$\int \mathrm{d}p_e^3 f(E_e, T) = N_e V = n_e \tag{2.33}$$

Here, the electron density N_e will ultimately determine the strength of the effective matter potential. To obtain the average effective Hamiltonian, project it on the electron states in Eq. 2.32 and integrate over the density and sum over the helicities:

$$\begin{aligned}
\langle H_{CC}\rangle &= \int \mathrm{d}p_e^3\, \langle e(p_e, h_e)| \times \frac{1}{2}\sum_{h_e} H f(E_e, T)\, |e(p_e, h_e)\rangle \\
&= \frac{G_F}{\sqrt{2}} \int \mathrm{d}p_e^3\, \langle e(p_e, h_e)| \left[\bar{\nu_e}\gamma^\rho \left(1-\gamma^5\right) \nu_e\right] f(E_e, T) \times \frac{1}{2}\sum_{h_e} \left[\bar{e}(x)\, \gamma_\rho \left(1-\gamma^5\right) e(x)\right] |e(p_e, h_e)\rangle \\
&= \frac{G_F}{\sqrt{2}} \bar{\nu_e}\gamma^\rho \left(1-\gamma^5\right) \nu_e \int \mathrm{d}p_e^3 f(E_e, T) \times \frac{1}{2}\sum_{h_e} \langle e(p_e, h_e)|\, \bar{e}(x)\, \gamma_\rho \left(1-\gamma^5\right) e(x)\, |e(p_e, h_e)\rangle \,.
\end{aligned} \tag{2.34}$$

First, calculate the sum using trace technology

$$\begin{aligned}\frac{1}{2}\sum_{h_e}\langle e(p_e,h_e)|\,\bar{e}(x)\,\gamma_\rho\,(1-\gamma^5)\,e(x)\,|e(p_e,h_e)\rangle &= \frac{1}{4E_eV}\sum_{h_e}\bar{u}_e^{h_e}(p_e)\,\gamma_\rho\,(1-\gamma^5)\,u_e^{h_e}(p_e)\\ &= \frac{1}{4E_eV}\,\mathrm{Tr}\left[\sum_{h_e}\bar{u}_e^{h_e}(p_e)u_e^{h_e}(p_e)\,\gamma_\rho\,(1-\gamma^5)\right]\\ &= \frac{1}{4E_eV}\,\mathrm{Tr}\left[(\not{p}_e+m_e)\,\gamma_\rho\,(1-\gamma^5)\right]\\ &= \frac{(p_e)_\rho}{E_eV}\,. \end{aligned} \tag{2.35}$$

Eq. 2.34 now becomes

$$\langle H_{CC}\rangle = \frac{G_F}{\sqrt{2}E_eV}\bar{\nu}_e\,(1-\gamma^5)\,\nu_e\int \mathrm{d}p_e^3\,\not{p}_e\,f(E_e,T)\,. \tag{2.36}$$

Expand the integral, and use the fact that $\vec{p}_e$ is odd:

$$\begin{aligned}\int \mathrm{d}p_e^3\,\not{p}_e\,f(E_e,T) &= \int \mathrm{d}p_e^3\,f(E_e,T)(\gamma^0E_e-\vec{p}_e\cdot\vec{\gamma})\\ &= \int \mathrm{d}p_e^3\,f(E_e,T)\gamma^0E_e\\ &= \gamma_0E_eN_eV\,.\end{aligned} \tag{2.37}$$

Inserting this into Eq. 2.36, we have

$$\begin{aligned}\langle H_{CC}\rangle &= \frac{G_FN_e}{\sqrt{2}}\bar{\nu}_e\,(1-\gamma^5)\,\nu_e\gamma_0\\ &= \sqrt{2}G_FN_e\bar{\nu}_{eE}\gamma^0\nu_{eL}\,,\end{aligned} \tag{2.38}$$

where the projection operator $(1-\gamma^5)$ in the first line ensures that only the left-hand compontent of the neutrino fields interact. Thus,

$$V_{CC} = \sqrt{2}G_FN_e\,,\quad H_{CC}\,|\nu_k\rangle = V_{CC}\,|\nu_k\rangle\,. \tag{2.39}$$

Here we see a crucial difference between the eigenvectors between the vacuum Hamiltonian defined in Eq. 2.16 and H_{CC}, namely that the CC interactions happen in the flavor basis rather than in the mass basis[3]. In other words, neutrinos propagate in their mass eigenstates, but interact in their flavor eigenstate. The mixing of mass eigenstates during propagation determines if the flavor eigenstate has oscillated or not. The interactions still conserve lepton number, but the kinetic Lagrangian will not.

For neutral current, we replace the electron field $e(x)$ in Eq. 2.31 by the fermion field $f(x)$, and the projection operator $(1-\gamma^5)$ with $(g_V^f-g_A^f\gamma^5)$. Again, the γ^5 will cause the spacial component of p_f to disappear after integration, and the only difference between the average effective Hamiltonian for the neutral current is then the factor g_V^f:

$$V_{NC}^f = \sqrt{2}G_FN_Ag_V^f\,. \tag{2.40}$$

Summing over the fermions, and assuming electrical neutrality and equal abundance of protons and neutrons, we have

$$\begin{aligned}V_{NC} &= \sum_{f\in e,p,n}V_{NC}^f\\ &= \sqrt{2}G_FN_A\sum_{f\in e,p,n}g_V^f\\ &= \sqrt{2}G_FN_A\left[-\frac{1}{2}+2\sin^2(\theta_W)+\frac{1}{2}-2\sin^2(\theta_W)-\frac{1}{2}\right]\\ &= -\frac{1}{\sqrt{2}}G_FN_e\,,\end{aligned} \tag{2.41}$$

where the electrical neutrality condition allows us to simply sum the vectorial couplings together, cancelling the electron and proton contributions (and hence, also the Weinberg angle dependence).

[3]A similar calculation for the NC reveals the same fact: neutrinos interact in the flavor basis.

2.2.5 Matter Oscillations

Since only ν_e undergo CC interactions in Earth-like matter, the V_{CC} potential is zero for all other flavors. However, since all flavors undergo NC interactions the total matter potential in matrix form is

$$V = \begin{bmatrix} V_{CC} + V_{NC} & 0 & 0 \\ 0 & V_{NC} & 0 \\ 0 & 0 & V_{NC} \end{bmatrix} = V_{CC}\,\delta_{\alpha e}\mathbb{1} + V_{NC}\mathbb{1}\,. \tag{2.42}$$

Just as in Eq. 2.18, we start with a Hamiltonian that solves the time-dependent Schrödinger equation. This time, let the Hamiltonian be

$$H = H_0 + H_I\,, \tag{2.43}$$

where H_0 is the Hamiltonian in vacuum, and H_I is our interaction Hamiltonian associated with our matter potentials. Let the wavefunction that describes the $\nu_\alpha \to \nu_\beta$ transition be denoted as

$$\psi_{\alpha\beta}(t) = \langle \nu_\beta | \nu_\alpha(t) \rangle\;, \tag{2.44}$$

i.e. the evolution of the state of a neutrino emitted at $t = 0$ with flavor α to flavor β at time t.

Now using Eq. 2.16 and Eq. 2.39, we are ready to see what form our Hamiltonians take. Let us start with the vaccum Hamiltonian H_0, and act on its Schrödinger equation with $\langle \nu_\beta |$:

$$i\frac{\mathrm{d}}{\mathrm{d}t}\,|\nu_\alpha(t)\rangle = H_0\,|\nu_\alpha(t)\rangle \implies i\frac{\mathrm{d}}{\mathrm{d}t}\psi_{\alpha\beta} = \langle \nu_\beta |\, H_0\, |\nu_\alpha(t)\rangle\;. \tag{2.45}$$

Reminding ourselves that the vacuum Hamiltonian H_0 has eigenstates in the mass basis, we write the following expression where use the relations Eq. 2.16 and Eq. 2.21 to switch between the flavor and mass basis with the PMNS elements:

$$\begin{aligned} \langle \nu_\beta |\, H_0 &= \sum_k U_{\beta k}\,\langle \nu_k |\, H_0 \\ &= \sum_k U_{\beta k} E_k\,\langle \nu_k | \\ &= \sum_\eta \sum_k U_{\beta k} E_k U^*_{\eta k}\,\langle \nu_\eta |\;. \end{aligned} \tag{2.46}$$

Thus,

$$\begin{aligned} \langle \nu_\beta |\, H_0\, |\nu_\alpha(t)\rangle &= \sum_\eta \sum_k U_{\beta k} E_k U^*_{\eta k}\,\langle \nu_\eta | \nu_\alpha(t)\rangle \\ &= \sum_\eta \sum_k U_{\beta k} E_k U^*_{\eta k}\psi_{\alpha\eta}(t)\,. \end{aligned} \tag{2.47}$$

Using the ultrarelativistic approximation from Eq. 2.24:

$$\begin{aligned} \sum_\eta \sum_k U_{\beta k} E_k U^*_{\eta k}\psi_{\alpha\eta}(t) &= \sum_\eta \sum_k U_{\beta k}\left(p + \frac{m_k^2}{2E}\right) U^*_{\eta k}\psi_{\alpha\eta}(x) \\ &= \sum_\eta \sum_k U_{\beta k}\left(p + \frac{m_k^2}{2E}\right) U^*_{\eta k}\psi_{\alpha\eta}(x)\,. \end{aligned} \tag{2.48}$$

Use the fact that $\sum_k m_k^2 = \sum m_1^2 +_k m_k^2 - m_1^2 = \sum_k m_1^2 + \Delta m_{k1}^2$ to pull out common terms out of the summation:

$$\begin{aligned} \sum_\eta \sum_k U_{\beta k}\left(p + \frac{m_k^2}{2E}\right) U^*_{\eta k}\psi_{\alpha\eta}(x) &= \sum_\eta \sum_k U_{\beta k}\left(p + \frac{m_1^2}{2E} + \frac{\Delta m_{k1}^2}{2E}\right) U^*_{\eta k}\psi_{\alpha\eta}(x) \\ &= \sum_\eta \sum_k \left(p + \frac{m_1^2}{2E}\right) U_{\beta k} U^*_{\eta k}\psi_{\alpha\eta}(x) + \sum_\eta \sum_k U_{\beta k}\frac{\Delta m_{k1}^2}{2E} U^*_{\eta k}\psi_{\alpha\eta}(x)\,. \end{aligned} \tag{2.49}$$

Unitarity gives $\sum_k U_{\beta k}U^*_{\eta k} = \delta_{\eta\beta}$, and the first term in the last step of Eq. 2.49 becomes

$$\sum_\eta \left(p + \frac{m_1^2}{2E}\right)\delta_{\beta\eta}\psi_{\alpha\eta}(x) = \left(p + \frac{m_1^2}{2E}\right)\psi_{\alpha\beta}(x)\,. \tag{2.50}$$

Our treatment of the interaction Hamiltonian is similar except for the fact that its eigenstates lie in the flavor basis, conviniently allowing us to letting it act directly on the flavor eigenstates:

$$\begin{aligned}\langle\nu_\beta|\, H_I &= V_\beta\,\langle\nu_\beta| \\ &= \delta_{\beta\eta}V_\beta\,\langle\nu_\eta|\;.\end{aligned} \tag{2.51}$$

Using Eq. 2.42 in component form, we rewrite this as

$$\begin{aligned}\delta_{\beta\eta}V_\beta\,\langle\nu_\eta| &= \delta_{\beta\eta}(V_{CC}\delta_{\beta e} + V_{NC})\,\langle\nu_\eta| \\ &= V_{CC}\delta_{\beta\eta}\delta_{\beta e}\,\langle\nu_\eta| + V_{NC}\,\langle\nu_\beta| \\ \implies \langle\nu_\beta|\,H_I\,|\nu_\alpha\rangle &= V_{CC}\delta_{\beta\eta}\delta_{\beta e}\,\langle\nu_\eta|\nu_\alpha\rangle + V_{NC}\,\langle\nu_\beta|\nu_\alpha\rangle \\ &= V_{CC}\delta_{\beta\eta}\delta_{\beta e}\psi_{\alpha\eta} + V_{NC}\psi_{\alpha\beta}\end{aligned} \tag{2.52}$$

Now, combining Eq. 2.49 and Eq. 2.52, we have for the full Hamiltonian

$$\langle\nu_\beta|\,H\,|\nu_\alpha(x)\rangle = \left(p + \frac{m_1^2}{2E} + V_{NC}\right)\psi_{\alpha\beta}(x) + \sum_\eta\sum_k\left(U_{\beta k}\frac{\Delta m^2_{k1}}{2E}U^*_{\eta k} + V_{CC}\delta_{\beta\eta}\delta_{\eta e}\right)\psi_{\alpha\eta}(x) \tag{2.53}$$

In this form, we see that the term $p + \frac{m_1^2}{2E} + V_{NC}$ is a common term to all flavor states, and does not affect the probability. It can be rotated away. Thus

$$\begin{aligned}\langle\nu_\beta|\,H\,|\nu_\alpha(x)\rangle &= \sum_\eta\sum_k\left(U_{\beta k}\frac{\Delta m^2_{k1}}{2E}U^*_{\eta k} + V_{CC}\delta_{\beta\eta}\delta_{\eta e}\right)\psi_{\alpha\eta}(x) \\ &= i\frac{\mathrm{d}}{\mathrm{d}x}\psi_{\alpha\beta}(x)\,.\end{aligned} \tag{2.54}$$

If we form the vector

$$\Psi_\alpha = \begin{pmatrix}\psi_{\alpha e}\\ \psi_{\alpha\mu}\\ \psi_{\alpha\tau}\end{pmatrix}\;, \tag{2.55}$$

we can write the Schrödinger equation on matrix form ($i\frac{\mathrm{d}}{\mathrm{d}x}\Psi_\alpha = H_F\Psi_\alpha$) and compare it with Eq. 2.54 to see that the flavor Hamiltonian takes the form

$$\begin{aligned}H_F &= \frac{1}{2E}(UM^2U^\dagger + A) \\ &= \frac{1}{2E}\left[U\begin{pmatrix}0 & 0 & 0\\ 0 & \Delta m^2_{21} & 0\\ 0 & 0 & \Delta m^2_{31}\end{pmatrix}U^\dagger\right] + \sqrt{2}G_F N_e\begin{pmatrix}1 & 0 & 0\\ 0 & 0 & 0\\ 0 & 0 & 0\end{pmatrix}\;.\end{aligned} \tag{2.56}$$

This is the three-flavor neutrino oscillation Hamiltonian that we will solve numerically to obtain the evolution of Ψ_α, whose squared components are the probabilities

$$\begin{aligned}P_\alpha = |\Psi_a|^2 &= \begin{pmatrix}|\psi_{\alpha e}|^2\\ |\psi_{\alpha\mu}|^2\\ |\psi_{\alpha\tau}|^2\end{pmatrix} \\ &= \begin{pmatrix}P_{\alpha e}\\ P_{\alpha\mu}\\ P_{\alpha\tau}\end{pmatrix}\end{aligned} \tag{2.57}$$

For $N_e = 0$, i.e. in vacuum, these probabilities are identical to the ones that we analytically derived in Eq. 2.28. For matter oscillations with $N_e \neq 0$, we do have closed form solutions, but they are not considered further here.

2.2.6 Two neutrino mixing

By working in the limit where one of the neutrino masses can be neglected, we can reduce the complexity of the analytical solution of neutrino oscillation. We now only consider the mixing between two neutrino flavors, say between ν_e, ν_μ, and ν_1, ν_2. In other words, we let $\Delta m^2_{31} = 0$.

The three-neutrino oscillation Hamiltonian from Eq. (2.56) now reduces to

$$\begin{aligned} H_F &= \frac{1}{2E}(UM^2U^\dagger + A) \\ &= \frac{1}{2E}\left[U\begin{pmatrix}0 & 0 & 0\\ 0 & \Delta m^2_{21} & 0\\ 0 & 0 & 0\end{pmatrix}U^\dagger\right] + \sqrt{2}G_F N_e\begin{pmatrix}1 & 0 & 0\\ 0 & 0 & 0\\ 0 & 0 & 0\end{pmatrix}\,. \end{aligned} \tag{2.58}$$

The rotation matrices R_{ij} that constitute U according to Eq. (2.12) can be simplified. The rotation R_{13} will not affect our mass matrix, since the former acts in the $1-3$ plane, and the latter sits in the $1-2$ plane. Thus, the reduced mass matrix $\mathcal{M}_{12}$ commutes with R_{13}. Analogously, the rotation matrix R_{23} also commutes with $\mathcal{M}_{12}$. Moreover, since $SO(3)$ is abelian, its generators commute, i.e.

$$[R_{ij}, R_{kl}] = R_{ij}R_{kl} - R_{kl}R_{ij} = 0\,. \tag{2.59}$$

Thus,

$$\begin{aligned} U\mathcal{M}_{12}U^\dagger &= R_{23}R_{13}R_{12}\mathcal{M}_{12}R^\dagger_{12}R^\dagger_{13}R^\dagger_{23} \\ &= R_{12}R_{23}R_{13}\mathcal{M}_{12}R^\dagger_{13}R^\dagger_{23}R^\dagger_{12} \\ &= R_{12}\mathcal{M}_{12}R_{23}R_{13}R^\dagger_{13}R^\dagger_{23}R^\dagger_{12}\,. \end{aligned} \tag{2.60}$$

And due to the fact that the rotation matrices are unitary,

$$R\,R^\dagger = \mathcal{I}\,, \tag{2.61}$$

we have that

$$\begin{aligned} U\mathcal{M}_{12}U^\dagger &= R_{12}\mathcal{M}_{12}R_{23}R_{13}R^\dagger_{13}R^\dagger_{12}R^\dagger_{23} \\ &= R_{12}\mathcal{M}_{12}R_{23}R^\dagger_{23}R^\dagger_{12} \\ &= R_{12}\mathcal{M}_{12}R^\dagger_{12}\,. \end{aligned} \tag{2.62}$$

We have now completely removed the dependence of the mixing angle between the ν_1 and ν_3 mass eigenstates, θ_{13}, and the dependece of the mixing angle between the ν_2 and ν_3 mass eigenstates, θ_{23}. We can see this clearly by writing our reduced mixing matrix, which is only constituted by the rotation in the $1-2$ plane, R_{12}.

$$U = R_{12}\begin{pmatrix}c_{12} & s_{12} & 0\\ -s_{12} & c_{12} & 0\\ 0 & 0 & 1\end{pmatrix} \tag{2.63}$$

Let us return to the Hamiltonian with our two-neutrino mixing matrix. We have

$$\begin{aligned} H_F &= \frac{1}{2E}\left[R_{12}\begin{pmatrix}0 & 0 & 0\\ 0 & \Delta m^2_{21} & 0\\ 0 & 0 & 0\end{pmatrix}R^\dagger_{12}\right] + \sqrt{2}G_F N_e\begin{pmatrix}1 & 0 & 0\\ 0 & 0 & 0\\ 0 & 0 & 0\end{pmatrix} \\ &= \frac{1}{2E}\left[\begin{pmatrix}c_{12} & s_{12} & 0\\ -s_{12} & c_{12} & 0\\ 0 & 0 & 1\end{pmatrix}\begin{pmatrix}0 & 0 & 0\\ 0 & \Delta m^2_{21} & 0\\ 0 & 0 & 0\end{pmatrix}\begin{pmatrix}c_{12} & s_{12} & 0\\ -s_{12} & c_{12} & 0\\ 0 & 0 & 1\end{pmatrix}^\dagger\right] + \sqrt{2}G_F N_e\begin{pmatrix}1 & 0 & 0\\ 0 & 0 & 0\\ 0 & 0 & 0\end{pmatrix}\,. \end{aligned} \tag{2.64}$$

We can reduce this down to two dimensions by extracting the upper-left block of all matrices. We now have the final two-neutrino Hamiltonian:

$$
\begin{aligned}
H_F &= \frac{1}{2E}\left[\begin{pmatrix} c_{12} & s_{12} \\ -s_{12} & c_{12}\end{pmatrix}\begin{pmatrix} 0 & 0 \\ 0 & \Delta m^2_{21}\end{pmatrix}\begin{pmatrix} c_{12} & s_{12} \\ -s_{12} & c_{12}\end{pmatrix}^\dagger\right] + \sqrt{2}G_F N_e \begin{pmatrix} 1 & 0 \\ 0 & 0\end{pmatrix} \\
&= \frac{1}{2E}\left[\begin{pmatrix} 0 & \Delta m^2_{21}s_{12} \\ 0 & \Delta m^2_{21}c_{12}\end{pmatrix}\begin{pmatrix} c_{12} & -s_{12} \\ s_{12} & c_{12}\end{pmatrix}\right] + \sqrt{2}G_F N_e \begin{pmatrix} 1 & 0 \\ 0 & 0\end{pmatrix} \\
&= \frac{1}{2E}\left[\begin{pmatrix} s^2_{12} + \sqrt{2}G_F N_e & \Delta m^2_{21}s_{12}c_{12} \\ \Delta m^2_{21}s_{12}c_{12} & \Delta m^2_{21}c^2_{12}\end{pmatrix}\right] \qquad (2.65)
\end{aligned}
$$

This matrix has eigenvalues which we identify as the effective two-neutrino squared-mass difference $(\Delta m^2_{21})^M$. They are

$$
\pm(\Delta m^2_{21})^M = \pm\sqrt{(\Delta m^2_{21}\cos(2\theta_{12}) - \sqrt{2}G_F N_e)^2 + (\Delta m^2_{21}\sin(2\theta_{12}))^2} \qquad (2.66)
$$

The matrix is diagonalized by the usual rotation matrix R_{12}, but with a different rotation angle. This now introduces the effective two-neutrino mixing angle θ^M_{12}:

$$
U^M = R^M_{12} = R_{12}(\theta^M_{12})\,. \qquad (2.67)
$$

U^M diagonalizes H_F if and only if

$$
\tan(2\theta^M_{12}) = \frac{\tan(2\theta_{12})}{1 - \frac{\sqrt{2}G_F N_e}{\Delta m^2_{21}\cos(2\theta_{12})}}\,. \qquad (2.68)
$$

Now assume that the matter density is sufficiently smooth along the trajectory x, that is $\mathrm{d}\theta_M/\mathrm{d}x \approx 0$. In its diagonalized form, the Schrödinger equation with two-neutrino Hamiltonian can be solved with this assuption. The solutions are the regular neutrino vacuum oscillations of Eq. (2.28) using $\theta[13] = \theta[23] = 0$, but with the effective parameters of Eqs. (**??**). That is

$$
P^M_{e\mu}(x) = \sin^2(2\theta^M_{12}))\sin^2(\frac{\Delta m^2_{21}x}{4E}) \qquad (2.69)
$$

2.2.7 Earth propagation

We now need to know how the electrons are distributed within the Earth. The Preliminary Earth Reference Model [4] gives us spherically symmetric piecewise polynomials for the Earth density in gcm^3 shown in the left panel of Fig. 2.3. We note a steep discontinuity at 3480 km where the density is nearly halved. This is the core-mantle boundary, and will be visible in our oscillations.

Using a value of $Y = 0.5$ electron per nucleon, we express the matter potential as

$$
\begin{aligned}
V_{CC} &= \sqrt{2}G_F N_e = \sqrt{2}G_F Y N_A\,\rho \\
&= 3.8\times 10^{-23}\,\mathrm{eVgcm}^{-3}\,, \qquad (2.70)
\end{aligned}
$$

a low number due to the smallness of G_F. This is plotted in the right panel of Fig. 2.3

Now, solving the Schrödinger equation with the Hamiltonian from Eq. 2.56 with the matter potential from the PREM, we obtain the nine combinations of probabilities through the Earth diameter. We note that due to our assumption of CP-invariance (and thus, T-invariance), the probabilities $P_{\alpha\beta}$ and $P_{\beta\alpha}$ are identically equivalent. The result for GeV neutrinos is shown in Fig. 2.4.

Now we need to incorporate the *zenith angle*, defined as the angle between the neutrino direction of travel and south. This way, neutrinos traveling through the entire diameter of the Earth up through the South Pole are defined as 'up-going', while neutrinos that start at the South Pole are 'down-going'. We will mostly work with the quantity $\cos(\theta_z)$. Since we are interested in the matter effects, we reserve our IceCube study to up-going neutrinos, i.e. neutrinos with zenith angle $-1 <= \cos(\theta_z) <= 0$. We now supplement our probability grid from Fig. 2.4 with the zenith dimension, allowing us to fully see the Earth matter effect on the oscillations in full. This is shown in Fig. 2.5.

The core-mantle boundary from Fig.2.3 is clearly displayed at $\cos(\theta_z) = -0.83$ as a sharp discontinuity for all flavors.

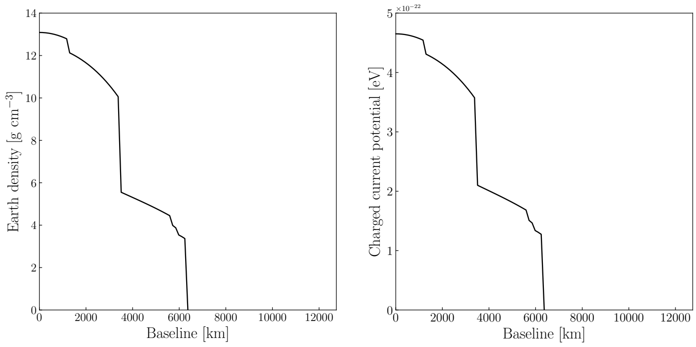

Figure 2.3: *Left panel:* The spherically symmetric Earth density according to PREM [4], as of distance from the core. *Right panel:* V_{CC} using the PREM density and 1/2 electrons per nucleon.

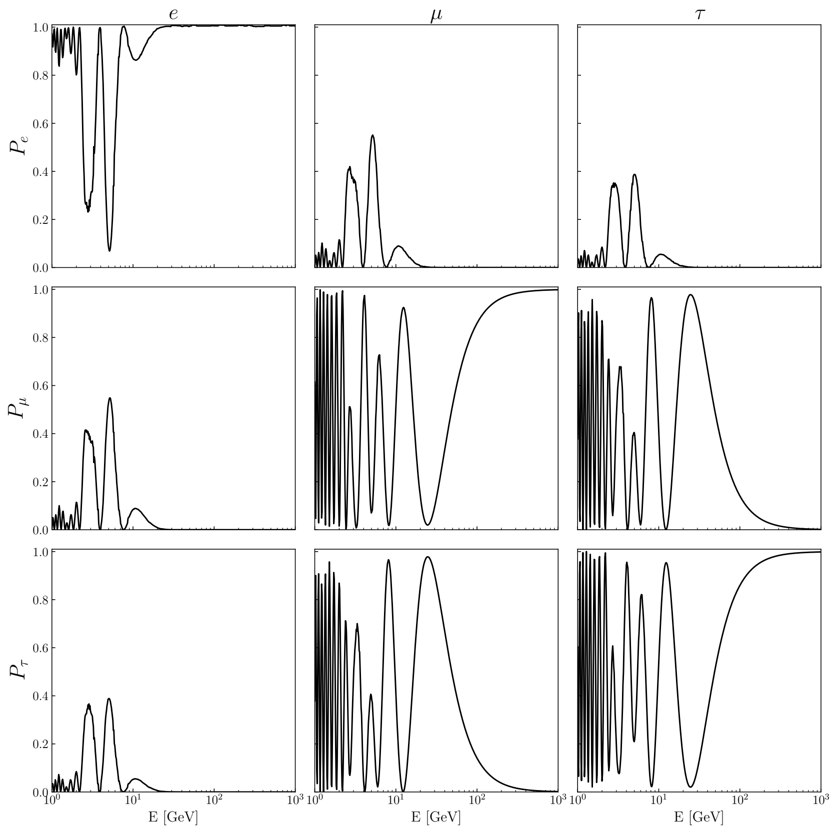

Figure 2.4

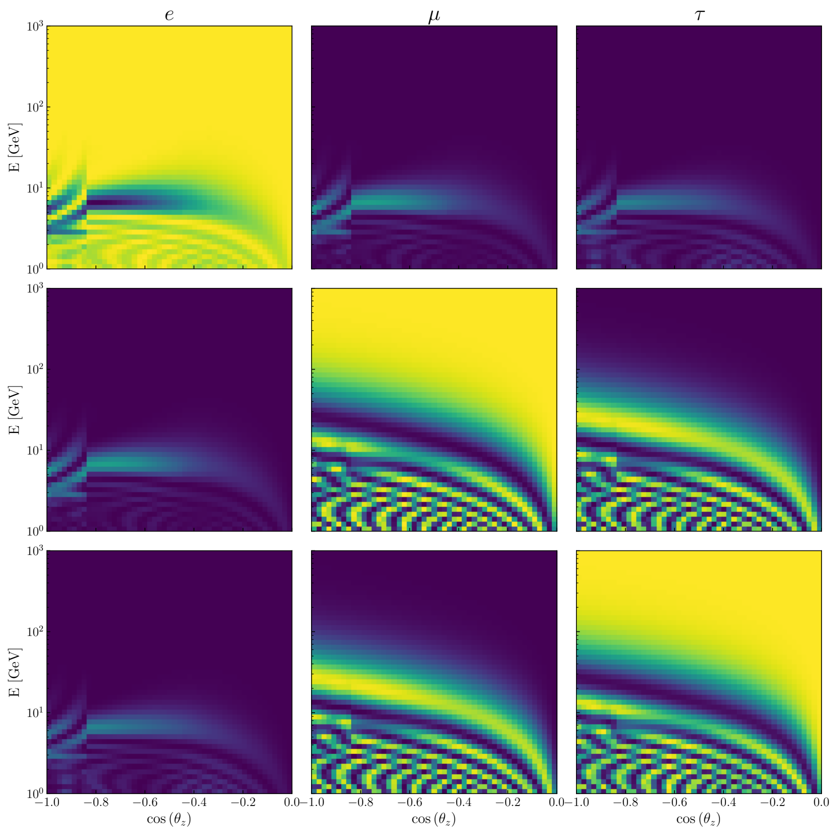

Figure 2.5: Oscillograms showing neutrino oscillations for all flavors in E-cos(θ_z) space.

Chapter 3

The Antarctic Detectors

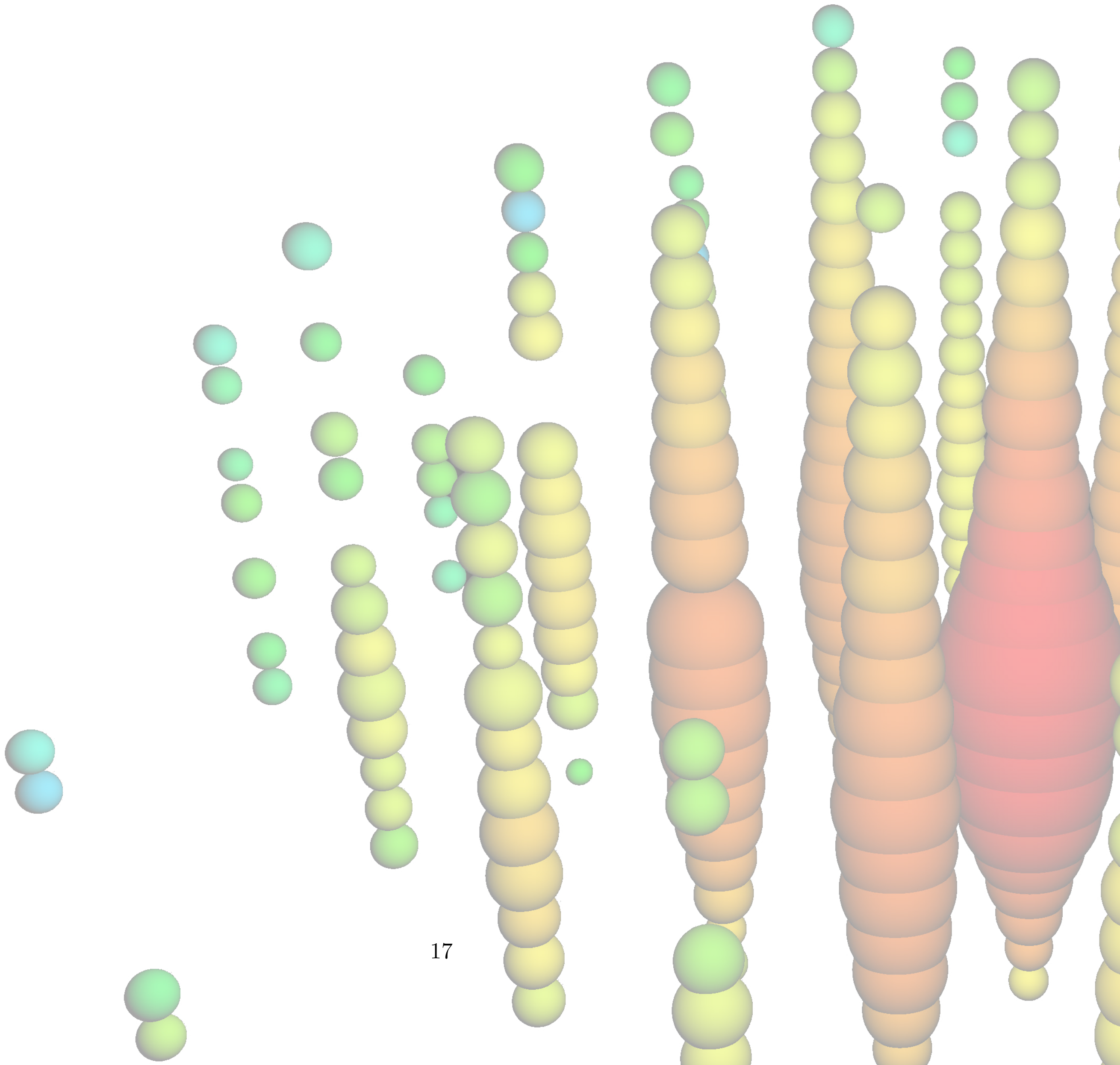

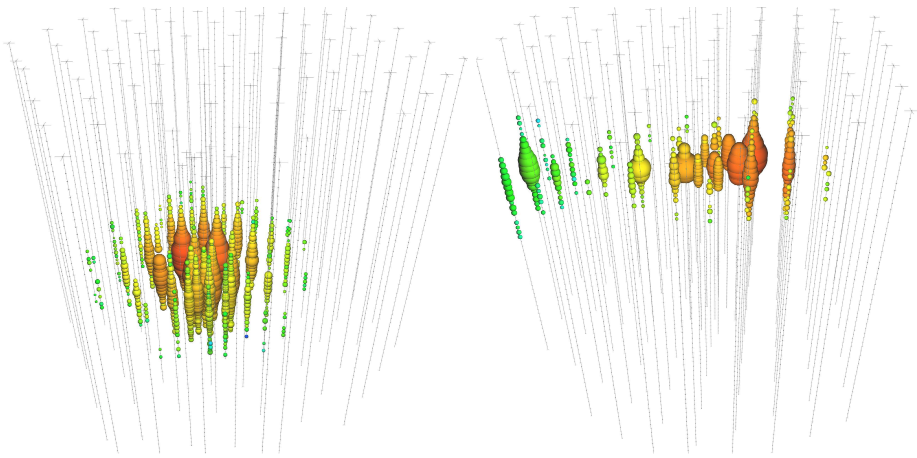

(a) Event classified as cascade (b) Event classified as track

Figure 3.1: The two event types distinguished in the IceCube detector.

3.1 Neutrino detection

We always observe neutrinos indirectly through their associated charged lepton. Regardless of the type of interaction (charged current via the W boson, or neutral current via the Z), a charged lepton exits with altered properties. The lepton is then detected, and the properties of the neutrino involved in the interaction is then deduced. This deduction is obviously imperfect, and this introduces complexities that we will handle in Ch. 3.2.

In this work, we only study the detectors handeled by the IceCube collaboration. They are of Cherenkov type, which means that they detect the secondary charged lepton by its emitted Cherenkov light, produced from its travel through the Antarctic ice. If the charged leptons interact heavily with the ice, they will travel a short distance and emit a localized flash of Cherenkov light. This event is referred to as a cascade. The neutral current interactions involves quarks, which recoils and procudes showers of hadrons. Also, charged current ν_e interactions also produce cascades. A cascade event is shown in Fig. 3.1a. If the charged leptons don't interact as much in the ice, they penetrate a larger part of it, emitting light and tertiary particles as they go. This event is referred to as a track, and are often due to muon charged current interactions. A track event is shown in Fig. 3.1b.

To detect the Cherenkov light, 60 Digital Optical Modules (DOMs) are placed on a long string up to 17 m apart. 86 of these strings are then lowered into 2.5 km deep boreholes in the ice. The holes are then sealed by refreezing the ice, resulting in a total of 5160 DOMs in a volume of approximately 1 km^3 [5].

The strings and DOMs are not spaced evenly, making some parts of the detector more sensitive to certain energy ranges than other. 8 strings packed more tightly than the other 78, making that part of the detector sensitive to neutrino energies down to single digit GeV. Due to this part being situated deep within the ice, it is referred to DeepCore. DeepCore will be treated as a separate and independent detector from the rest, which retains the name IceCube. A view of the current setup can be seen in Fig. **??**. In this work, we consider DeepCore data between 5.6 GeV to 56 GeV and IceCube data in the range 0.5 TeV to 10 TeV.

In 2017, the PINGU Letter of Intent was published [6]. The 'Precision IceCube Next Generation Upgrade' is an upgrade that will supplement DeepCore, i.e. boosing the capabilites of neutrino detection at the GeV scale. As the PINGU upgrade is not yet financed nor built, we are not able to use any data from it. However, the collaboration has released preliminary simulations which we will use to see how the upgrade might improve IceCube and DeepCore bounds. The PINGU simulations have the same structure as the DeepCore data, so any analysis referring to DeepCore will also apply to PINGU except where noted. However, we treat the PINGU detector as independent of the DeepCore experiment.

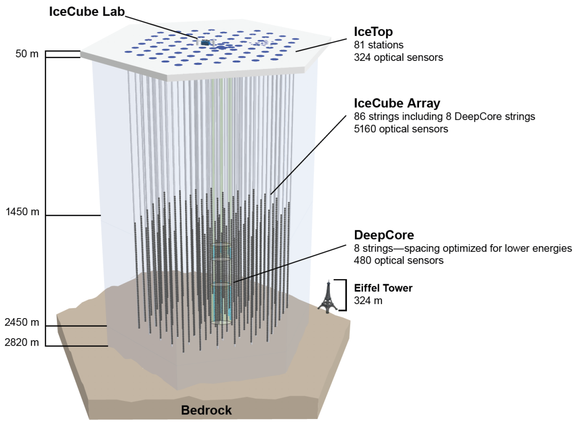

Figure 3.2: View of the full IceCube array

3.1.1 Atmospheric Neutrino Flux

Atmospheric neutrinos originates from cosmic rays composed of protons interacting with nuclei in the atmosphere. These interactions ultimately produces pions, which decay as

$$\begin{aligned} &\pi^+ \to \mu^+ + \nu_\mu\,, \quad \pi^- \to \mu^- + \bar{\nu}_\mu \\ &\pi^+ \to e^+ + \nu_e\,, \quad\; \pi^- \to e^- + \bar{\nu}_e\,. \end{aligned} \tag{3.1}$$

In the muonic decay channel, muons are emitted which will be detected by the IceCube detector. A part of the uncorrelated systematic error comes from this *muon background*, i.e. events misclassified as muons from ν_μ interactions rather than from pion decay. Moreover, the atmospheric flux is often associated with a large error. In this work, we will use a flux normalization error of 24%, and a zenith slope error of 4% [9].

The flux is provided in [10, 7], and a selection is shown in Table **??** The flux data is binned in $\cos(\theta_z^{true})$. The fluxes are averaged over azimuthal direction and over solar minimum/maximum. The units of the fluxes are given as $\mathrm{GeV}^{-1}\,\mathrm{m}^{-2}\,\mathrm{s}^{-1}\,\mathrm{sr}^{-1}$ and are omitted from the table for clarity. We note that the fluxes for ν_τ and $\nu_{\bar{\tau}}$ are missing. Kaons can decay into neutral pions, which in turn can produce ν_τ, but this branching ratio is extremely small. Thus, we never have to use probabilities on the form $P_{\tau\beta}$, since we have no incoming atmospheric ν_τ flux. Interpolating the data yields makes us capable of returning all four necessary fluxes for a given true energy and true zenith. The result is shown in Fig. **??**.

E^{true} [GeV]	ϕ_μ	$\phi_{\bar{\mu}}$	ϕ_e	$\phi_{\bar{e}}$	$\cos(\theta_z^{true})$
27825	6.06×10^{-12}	3.17×10^{-12}	1.56×10^{-13}	1.04×10^{-13}	[-0.2, -0.1]
247707	5.94×10^{-16}	2.92×10^{-16}	1.36×10^{-17}	8.12×10^{-18}	[-0.7, -0.6]
22	3.33×10^{-2}	2.78×10^{-2}	9.57×10^{-3}	7.15×10^{-3}	[-0.3, -0.2]
432876	5.19×10^{-17}	2.32×10^{-17}	1.46×10^{-18}	9.83×10^{-19}	[-1.1, -1.0]
64280	1.58×10^{-13}	8.10×10^{-14}	3.49×10^{-15}	2.21×10^{-15}	[-0.4, -0.3]

Table 3.1: A selection of processed atmospheric South Pole fluxes from [10] by Honda et al. [7].

3.1.2 Event Reconstruction

After an event has occurred, the IceCube algorithms process the data coming from the detector to *reconstruct* the event. This means that, given the parameters recorded by the detector, what are their "true" values? We are interested in two variables: the energy and the direction. Each event is tagged with a probable energy and zenith angle, called the recostructed parameters E^{reco} and $\cos(\theta_z^{reco})$, which are the parameters according to the DOMs. The collaboration then uses numerous sophisticated methods to

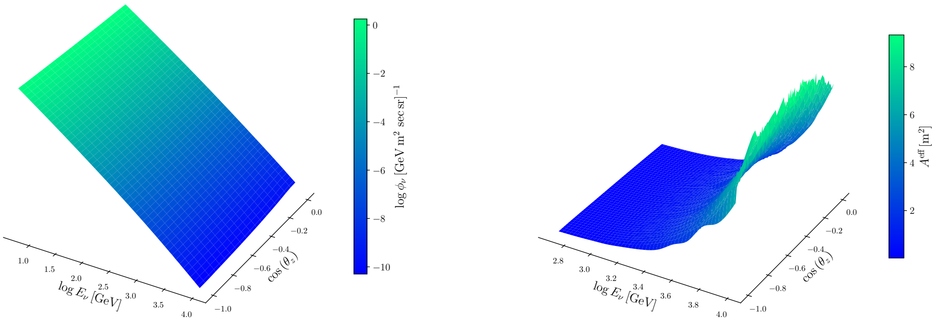

Figure 3.3: *Left panel:* Interpolated South Pole atmospheric flux with data from [7]. *Right panel:* Interpolated IceCube effective area with data from [8].

backtrack the reconstructed parameters to the true parameters. So a charged lepton hits the DOMs, and we ultimately end up with the associated neutrino's true and reconstructed energy and zenith angle. The reconstructed parameters are what we are using to analyze the data (because this is what the detector actually sees), while the true parameters are used in the determination of that neutrino's 'actual' flux and cross-section (because this is what Nature sees).

How do we then translate between the reconstructed and true parameters? In this work, we are using two different methods, which are based on the form of data available to us. They will be outlined in Sec.3.2 and Sec. 3.3.

3.2 IceCube

As the neutrinos have propagated the Earth, they arrive at the South Pole, where they interact with charged lepton in the ice. We now are interested in the effective area A^{eff}, i.e. the cross-section of the detector that the lepton is exposed to. A^{eff} depends on several parameters, some of them being detector physical volume, E^{true}, $\cos(\theta_z^{true})$ and the neutrino cross-section. Fortunately, the binned A^{eff} is provided to us by the collaboration [8]. The data file has the following form

E_{min}^{true} [GeV]	E_{max}^{true} [GeV]	$\cos(\theta_z^{true})_{min}$	$\cos(\theta_z^{true})_{max}$	A^{eff} [m^2]
251	316	-0.92	-0.91	0.0174
794300	1000000	-0.80	-0.79	69.3600
3981	5012	-0.78	-0.77	3.1490
1585	1995	-0.07	-0.06	0.4659
398	501	-0.73	-0.72	0.0555

Table 3.2: IceCube-86 effective area from [8]

Here, A^{eff} has been averaged over A_μ^{eff} and $A_{\bar{\mu}}^{\text{eff}}$. Just as with the fluxes, we interpolate this in E^{true}, $\cos(\theta_z^{true})$ and show the result

So now we have the physical quantities in the true parameters. But as we discussed, we need a way to translate this into the reconstructed parameters that the detector gives us. We will call the relationship between E^{reco} and E^{true} the energy resolution function, and the relationshop between $\cos(\theta_z^{reco})$ and $\cos(\theta_z^{true})$ the zenith resolution function. We assume the relationship to follow a logarithmic Gaussian distribution, giving it the form

$$R(x^r, x^t) = \frac{1}{\sqrt{2\pi}\sigma_{x^r} x^r} \exp\left[-\frac{(\log x^r - \mu(x^t))^2}{2\sigma_{x^r}^2}\right] . \tag{3.2}$$

The parameters of the Gaussian are $\sigma_{x^r}(x^t)$ and $\mu(x^t)$, which are functions of the true parameters. By multiplying the Gaussian in Eq. 3.2, we are reweighing the values by the probability density of that point. This process is also called *smearing* because it effectively spreads out the data around a certain point.

So how do we then obtain $\sigma_{x^r}(x^t)$ and $\mu(x^t)$ needed to construct the Gaussian? A Monte Carlo sample publically released by the collaboration has all the ingredients that we need [11]. In Table. **??** we show a selection of the data. The "pdg" column refers to the Monte Carlo particle classification, where 13 is the tag for ν_μ, while -13 refers to an $\bar{\nu}_\mu$. Here we note a crucial property of the IceCube dataset that will impact our analysis: the MC released by the collaboration only includes simulated muon events.

pdg	E^{reco} [GeV]	$\cos(\theta_z^{reco})$	E^{true} [GeV]	$\cos(\theta_z^{true})$
13	1665	-0.645884	592	-0.653421
13	587	-0.373241	342	-0.424979
-13	1431	-0.177786	1169	-0.189949
-13	831	-0.807226	1071	-0.805559
13	988	-0.370746	1861	-0.367922

Table 3.3: A selection of the data found in **??**

First, we let $\cos(\theta_z^{reco}) = \cos(\theta_z^{true})$ for all values. The angular resolution in IceCube for track-like events is less than 2°, making $\cos(\theta_z^{true})$ coincide with $\cos(\theta_z^{reco})$ for our study [12]. Thus, we only need to concern ourselves with the energy resolution. In Fig. 3.4, we have plotted all event counts found in the MC file, over 8 million. However, this is too much data to process efficiently, with many outliers that ultimately don't weigh in that much in the final event count. To resolve this, we have opted to train a Gaussian process regressor on the dataset, from which we can extract the predicted mean and standard deviation for a point. When doing this over E^{reco}, we sample E^{true} in the 99th percentile around the predicted mean. We then obtain the shaded band shown in Fig. 3.4.

The event rate for each bin reads

$$N_{ij} = T \sum_\beta \int_{(\cos\theta_z^r)_i}^{(\cos\theta_z^r)_{i+1}} \mathrm{d}\cos\theta_z^r \int_{E_j^r}^{E_{j+1}^r} \mathrm{d}E^r \int_0^\pi R(\theta^r, \theta^t)\mathrm{d}\cos\theta^t \int_0^\infty R(E^r, E^t)\phi_\beta^{\text{det}} A_\beta^{\text{eff}} \mathrm{d}E^t \,, \tag{3.3}$$

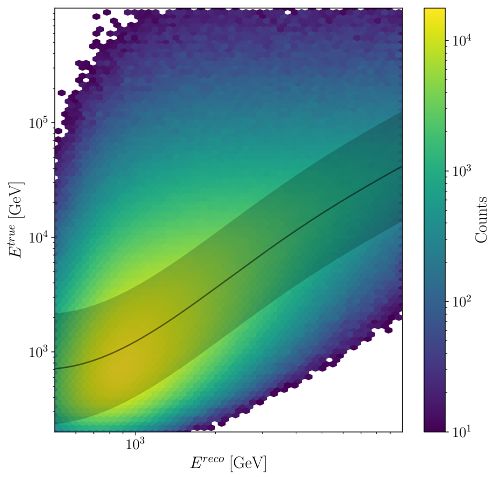

Figure 3.4: Relationship between the true and reconstructed muon energy in the IceCube MC sample [11]. Shaded area shows the 99.9th percentile limits predicted by the regressor trained on this set.

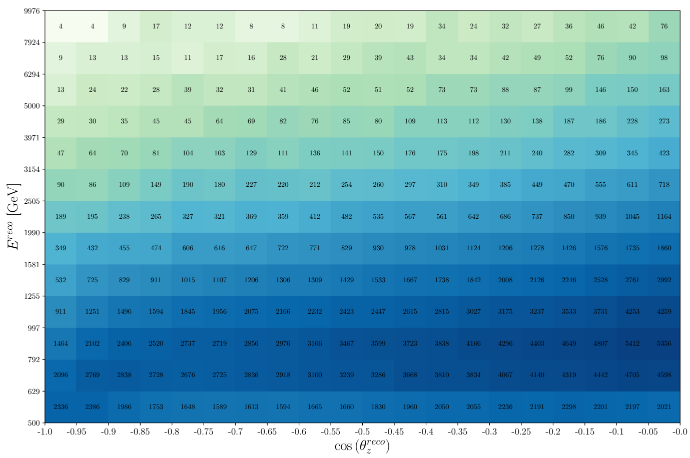

Figure 3.5: IceCube track events from [12].

where T is the live time of the detector. Now this expression handles the Gaussian smearing, but we are not provided systematic error sources, DOM efficiencies, and many more nuisance parameters. To correct this, we will aim to come as close as possible to the IceCube Monte Carlo, and then normalize with it. That way, we know that our null hypotheses will align while we are free to form additional hypotheses with different physics parameters. The binned Monte Carlo events that IceCube used as their null hypothesis in the 2020 sterile analysis is shown in

The latest available data collected and processed by the collaboration contains 305,735 muon track events, collected over eight years [12].

Monte Carlo normalization

Independent researchers outside of the IceCube collaboration will not be able to more percisely simulate the detector. The IceCube Monte Carlo is a complex and proprietary machinery, so our goal in this section is to come as close as we can to their Monte Carlo simulations. After we are confident that our code displays the same overall features as the 'offical', we normalize our results N_{ij}^{sim} as

$$N_{ij} = \frac{N_{ij}^{\text{null}}}{N_{ij}^{\text{MC}}} N_{ij}^{\text{sim}} \,. \tag{3.4}$$

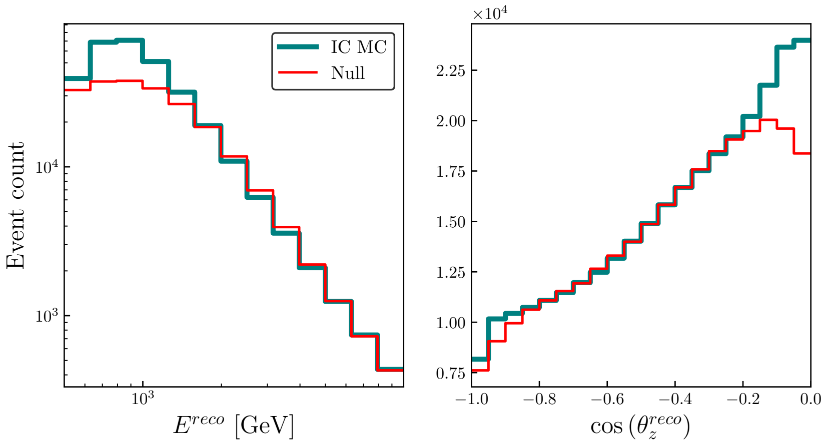

Figure 3.6: IceCube Monte Carlo, binned in E^{reco} and $\cos(\theta_z^{reco})$. We compare this with our simulations shown as 'Null' in the plots.

For each bin i, j, we then obtain a correction factor which contains information that we are unable to obtain or sufficiently incorporate. One example of such information is the systematic errors of the DOMs. Recent IceCube data releases do not include such information. Since the systematic errors are affecting the event count on a bin-by-bin basis, they can in theory drastically modify the binned results. Another example of an error source what will be remedied by this method is the flux. We are using a fairly simple model of the atmospheric flux that excludes atmospheric prompt and astrophysical fluxes. The IceCube collaboration use several different flux models which are initialized by a parametrization of the cosmic ray flux.[1]

In Fig. 3.6, we present the Icecube Monte Carlo obtained from their 2020 sterile analysis [12], along with our null hypothesis times a constant factor. We deemed these shapes to be satisfactory, thus allowing us to multiply Eq. 3.3 by the correction factors of Eq. 3.4. We now arrive to our final event count

$$N_{ij} = \frac{N_{ij}^{\text{null}}}{N_{ij}^{\text{MC}}} T \sum_{\beta} \int_{(\cos\theta_z^r)_i}^{(\cos\theta_z^r)_{i+1}} \mathrm{d}\cos\theta_z^r \int_{E_j^r}^{E_{j+1}^r} \mathrm{d}E^r \int_{E_{min}^t}^{E_{max}^t} R(E^r, E^t) \phi_\beta^{\text{det}} A_\beta^{\text{eff}} \, \mathrm{d}E^t \,, \tag{3.5}$$

with E_{min}^t, E_{max}^t, and $R(E^r, E^t)$ taken from the Gaussian process regressor. Thus, we are now able to sufficiently approximate the IceCube Monte Carlo, which makes us able to run simulations based on different physics scenarios.

[1] Included in the cosmic ray models are e.g. the pion to kaon ratio, which are often used as a nuisance parameter. By not being able to include this in our error analysis, our method will be limited to only consider the overall flux normalization, rather than the components that produce the flux in the first place.

3.3 DeepCore

In this part, we use the publically available DeepCore data sample [13] which is an updated version of what was used by the IceCube collaboration in a ν_μ disappreearance analysis [14].

The detector systematics include ice absorption and scattering, and overall, lateral, and head-on optical efficiencies of the DOMs. They are applied as correction factors using the best-fit points from the DeepCore 2019 ν_τ appearance analysis [15].

The data include 14901 track-like events and 26001 cascade-like events, both divided into eight $\log_{10} E^{reco} \in [0.75, 1.75]$ bins, and eight $\cos(\theta_z^{reco}) \in [-1, 1]$ bins. Each event has a Monte Carlo weight $w_{ijk,\beta}$, from which we can construct the event count as

$$N_{ijk} = C_{ijk} \sum_\beta w_{ijk,\beta} \phi_\beta^{\text{det}} \,, \tag{3.6}$$

where $C_{k\beta}$ is the correction factor from the detector systematic uncertainty and ϕ_β^{det} is defined as Eq. **??**. We have now substituted the effect of the Gaussian smearing by treating the reconstructed and true quantities as a migration matrix.

The oscillation parameters used on our DeepCore simulations are from the best-fit in the global analysis in [3]: $\theta_{12} = 33.44°$, $\theta_{13} = 8.57°$, $\Delta m_{21}^2 = 7.42\,\text{eV}^2$, and we marginalize over Δm^2 and θ_{23}.

3.4 PINGU

The methodology behind the PINGU simulations are the same as with our DeepCore study . We use the public MC [16], which allows us to construct the event count as in Eq. 3.6. However, since no detector systematics is yet modelled for PINGU, the correction factors C_{ijk} are all unity. As with the DeepCore data, the PINGU Monte Carlo is divided into eight $\log_{10} E^{reco} \in [0.75, 1.75]$ bins, and eight $\cos(\theta_z^{reco}) \in [-1, 1]$ bins for both track- and cascade-like events. We generate 'data' by predicting the event rates at PINGU with the following best-fit parameters from [3], except for the CP-violating phase which is set to zero for simplicity.

$$\begin{aligned}
&\Delta m_{21}^2 = 7.42 \times 10^{-5}\,\text{eV}^2, \;\; \Delta m^2 = 2.517 \times 10^{-3}\,\text{eV}^2, \\
&\theta_{12} = 33.44°, \quad \theta_{13} = 8.57°, \quad \theta_{23} = 49.2°, \quad \delta_{\text{CP}} = 0\,.
\end{aligned} \tag{3.7}$$

Chapter 4

Beyond the 3ν Picture

$$\mathcal{L}_{\mathrm{NC}} = -2\sqrt{2}G_F\epsilon_{\alpha\beta}^{fX}\left(\bar{\nu}_\alpha\gamma^\mu P_L\right.$$

4.1 The Sterile State

In 1996, the LSND experiment reported an excess of $\bar{\nu}_e$ events from an $\bar{\nu}_\mu$ beam [17]. Nine years later, MiniBooNE not only reproduced the $\bar{\nu}_e$ anomaly, but observed an excess in the ν_e events too. Together with the so-called reactor and gallium anomalies, these reports suggested that the three massive neutrino framework could be amended. By introducing a fourth heavy mass state ν_4, both appearance and disappeareance anomalies could be minimally accomodated. However, we know from the decay width of the Z boson that it only can interact with three flavor species[1], so this fourth mass state cannot be interacting weakly. In other words, it needs to transform as a singlet under the broken gauge group $SU(2)_L \times U(1)_{EM}$. We now distinguish between the three original neutrino flavors (e, μ, and τ) and the new fourth flavor by calling the former *active* neutrinos and the latter *sterile* due to its non-interacting behavior.

The experiments listed above indicate that the mass-squared difference of the sterile neutrino is in the eV^2 scale, while the two others are three and five magnitudes smaller. To remind us of this hierarchy, we write $3+1$, since the sterile state proposed is a lot more massive than the active states.

Two neutrino physics parameters probed by CMB lensing observations are the effective number of neutrinos N_{eff}, and the sum of neutrino masses $\sum m_i$. The 2018 results from the Planck Collaboration in [19] constrain the parameters to

$$N_{\text{eff}} = 2.96^{+0.34}_{-0.33}\,, \quad \sum m_i < 0.12\,\text{eV} \quad (95\%)\,, \tag{4.1}$$

consistent with the Standard Model with oscillations[2] prediction of $N_{\text{eff}} = 3.045$ degrees [20]. Assuming the Planck data, one thermalized sterile neutrino ($N_{\text{eff}} = 4$) is excluded at 6σ. Thus, thermalized sterile neutrinos are strongly in tension with cosmological observations if one does not consider some special mechanism. So if a fourth neutrino species is present in nature, it will have ramifications not only on neutrino physics itself, but on our understanding of the CMB aswell.

4.1.1 The Hamiltonian

The inclusion of the sterile state in the Hamiltonian is straightforward. We extend the PMNS matrix with terms for the mixing between the new flavor (U_{si}) and mass ($U_{\alpha 4}$) eigenstates:

$$U_{4gen} = \begin{pmatrix} U_{e1} & U_{e2} & U_{e3} & U_{e4} \\ U_{\mu 1} & U_{\mu 2} & U_{\mu 3} & U_{\mu 4} \\ U_{\tau 1} & U_{\tau 2} & U_{\tau 3} & U_{\tau 4} \\ U_{s1} & U_{s2} & U_{s3} & U_{s4} \end{pmatrix}, \tag{4.2}$$

where a common parametrization of this new mixing matrix is

$$U_{4gen} = R_{34} R_{24} R_{14} U_{3gen}\,. \tag{4.3}$$

This parametrization does not affect the physics, but determines the structure of the mixing angles.

The mass matrix extends analogously:

$$M^2_{4gen} = \begin{pmatrix} 0 & 0 & 0 & 0 \\ 0 & \Delta m^2_{21} & 0 & 0 \\ 0 & 0 & \Delta m^2_{31} & 0 \\ 0 & 0 & 0 & \Delta m^2_{41} \end{pmatrix}. \tag{4.4}$$

Now, the interaction with matter requires a careful reconsideration of the matter potential. We start off with the unaltered potential matrix from Eq. 2.42. Just as with the PMNS matrix, we extend this to 4×4:

$$\begin{pmatrix} V_{CC} + V_{NC} & 0 & 0 & 0 \\ 0 & V_{NC} & 0 & 0 \\ 0 & 0 & V_{NC} & 0 \\ 0 & 0 & 0 & 0 \end{pmatrix}. \tag{4.5}$$

Now we need to include the terms that describes the matter potential felt by the sterile flavor state. Recalling our discussion above, we remind ourselves that the sterile neutrino by definition does not

[1] Direct measurements of the invisible Z decay yields $N = 2.92 \pm 0.05$ [18].

[2] Of course, the Standard Model *without* neutrino masses dictates $N_{\text{eff}} = 3$ and $\sum m_i \equiv 0$.

participate in any interaction[3]. Thus, all potential terms involving the sterile state are zero. In other words, the potential matrix in Eq. 4.5 is complete, save for the usual subtraction by a constant times the identity matrix:

$$\begin{aligned} V_{4gen} &= \begin{pmatrix} V_{CC}+V_{NC} & 0 & 0 & 0 \\ 0 & V_{NC} & 0 & 0 \\ 0 & 0 & V_{NC} & 0 \\ 0 & 0 & 0 & 0 \end{pmatrix} - V_{NC} \begin{pmatrix} 1 & 0 & 0 & 0 \\ 0 & 1 & 0 & 0 \\ 0 & 0 & 1 & 0 \\ 0 & 0 & 0 & 1 \end{pmatrix} = \sqrt{2}G_F \begin{pmatrix} N_e & 0 & 0 & 0 \\ 0 & 0 & 0 & 0 \\ 0 & 0 & 0 & 0 \\ 0 & 0 & 0 & -N_n/2 \end{pmatrix} \\ &= \sqrt{2}G_F N_e \begin{pmatrix} 1 & 0 & 0 & 0 \\ 0 & 0 & 0 & 0 \\ 0 & 0 & 0 & 0 \\ 0 & 0 & 0 & -1/2 \end{pmatrix}. \end{aligned} \tag{4.6}$$

where we have assumed electrical neutrality in the last step, yielding $N_e = N_n$.

Thus, the final Hamiltonian with a fourth sterile neutrino is

$$H_{4gen} = \frac{1}{2E}\left[U \begin{pmatrix} 0 & 0 & 0 & 0 \\ 0 & \Delta m^2_{21} & 0 & 0 \\ 0 & 0 & \Delta m^2_{31} & 0 \\ 0 & 0 & 0 & \Delta m^2_{41} \end{pmatrix} U^\dagger \right] + \sqrt{2}G_F N_e \begin{pmatrix} 1 & 0 & 0 & 0 \\ 0 & 0 & 0 & 0 \\ 0 & 0 & 0 & 0 \\ 0 & 0 & 0 & -1/2 \end{pmatrix}. \tag{4.7}$$

Now, looking at Eqs. 4.3 and 4.4, we see that we have introduced four new parameters: Δm^2_{41}, θ_{14} , θ_{24}, θ_{34}. In our analysis, we reduce the number of parameters by only considering Δm^2_{41} and θ_{24}, which are the most important for the ν_μ oscillations. In fact, one can close the e channel by letting $\theta_{14} = 0$ in the GeV to TeV range, thus using a two-flavor neutrino approximation. This is not done in this work.

4.1.2 Sterile Signals

Since the new neutrino does not interact weakly, how do we then detect its signal? If the sterile mixing angle θ_{i4} is non-zero, we allow the sterile mass state to mix with the active state i. The most interesting case is when $\theta_{24} \neq 0$, which for $\Delta m^2_{41} \sim \mathrm{eV}^2$ gives rise to a resonant disappeareance in the for $P_{\bar{\mu}\bar{\mu}}$, shown in Fig. 4.1a.

So for a eV-scale sterile neutrino and a non-zero θ_{24}, we expect a TeV $\bar{\nu}_\mu$ disappearance. The resonance dip is affected by the value of Δm^2_{41} and θ_{24} as shown in Fig. 4.1b. We see how the value of Δm^2_{41} shifts the peak, while the mixing angle adjusts its strength. In the $3+0$ scenario, $P_{\bar{\mu}\bar{\mu}} = 1$ in this range. Thus, if we are able to see a $\bar{\nu}_\mu$ disappearance in the TeV region, we are in a good position to argue for a eV scale Δm^2_{41}.

[3]The exception to this is of course gravity. The sterile neutrino is not massless.

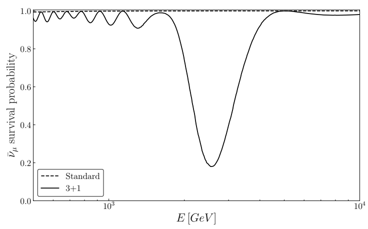

(a) $P_{\bar{\mu}\bar{\mu}}$ resonant disappearance

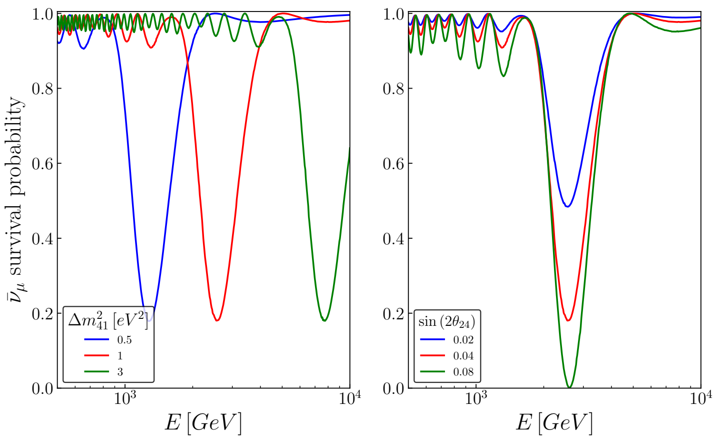

(b) Shifting and amplification of the resonance by altering Δm^2_{41} and θ_{24}, respectively.

4.2 Non-Standard Interactions

We have no reason to believe that the Standard Model gauge group is the complete picture. We have already seen how the failure of the Standard Model to predict neutrino masses and flavor osillations forces us to amend it. Just as the electroweak theory $SU(2)_L \times U(1)_Y$ is spontaneously broken to $U(1)_{EM}$, a higher order theory at a different energy scale with completely different properties might undergo a similar spontaneous symmetry break at high energies, producing at lower energies the Standard Model that we know. In fact, just as the fermion masses originate from the electroweak symmetry breaking, the neutrino masses might be generated from another broken symmetry resulting in the Standard Model gauge group. In this sense, the Standard Model might be considered an effective low energy theory, which is yiels impressive results in some areas, but failing in others.

Compared to other fermions, the lightness of neutrino masses[4] along with their sparse SM interactions might indicate that these particles provide the best starting point for us to probe new physics, in which exotic neutrino interactions might occur [21]. We call these interactions non-standard interactions (NSI) in order to distinguish them from the 'standard' interactions of the Standard Model.

Following the approach of the Standard Model that the group generators uniquely determine the gauge bosons, a different gauge theory will have different interactions than those we presently know. These new interactions can be parametrized as model-independent four-fermion effective operators [22, 23]. Following the discussion in [24], we see that the NSI parameters ϵ resulting from six-dimensional operators have the scale

$$\epsilon \propto \frac{m_W^2}{m_\epsilon^2} \sim \frac{10^{-2}}{m_\epsilon^2} \tag{4.8}$$

in TeV, so the new interactions generated at a mass scale of $m_\epsilon = 1\,\text{TeV}$ will produce parameters in the order of 10^{-2}, two magnitudes below the standard matter effect. Thus, if we assume the new interactions to arise from a higher-energy theory above electroweak scale, we then predict that the parameters contribute with at most a factor of 10^{-2} to the standard matter effect, decreasing quadratically.

4.2.1 Altering the Matter Potential

Up until now, we have only considered weak neutrino interactions with electrons, protons, and neutrons. We can phenomenologically allow these interactions to include the up and down quarks which are present in the Earth as the fundamental components of neutrons and protons, as seen in the Lagrangians

$$\begin{aligned}
\mathcal{L}_{\text{CC}} &= -2\sqrt{2}G_F \epsilon_{\alpha\beta}^{ff'X} \left(\bar{\nu}_\alpha \gamma^\mu P_L \ell_\beta\right) \left(\bar{f}' \gamma_\mu P_X f\right) \\
\mathcal{L}_{\text{NC}} &= -2\sqrt{2}G_F \epsilon_{\alpha\beta}^{fX} \left(\bar{\nu}_\alpha \gamma^\mu P_L \nu_\beta\right) \left(\bar{f} \gamma_\mu P_X f\right) ,
\end{aligned}$$

where CC denotes the charged current interaction with the matter field $f \neq f' \in \{u, d\}$, and NC denotes the neutral current interaction with $f \in \{e, u, d\}$. The CC NSI effect affects neutrino production and detection, and will not be considered further. NC NSI affect the matter potential, and is thus of interest to us.

We have no independent sensitivity for the neither chirality nor flavor type of ϵ^X, so we sum over these and study the effective matter NSI parameter $\epsilon_{\alpha\beta}$:

$$\epsilon_{\alpha\beta} = \sum_{X \in \{L,R\}} \sum_{f \in \{e,u,d\}} \frac{N_f}{N_e} \epsilon_{\alpha\beta}^{fX} . \tag{4.9}$$

Our matter study will be wholly confined to the interior of the Earth, where we assume electrical neutrality and equal distribution of neutrons and protons, we get $N_u/N_e \simeq N_d/N_e \simeq 3$. Also we assume the components $\epsilon_{\alpha\beta}$ to be real. Thus,

$$\epsilon_{\alpha\beta} = \sum_X \epsilon_{\alpha\beta}^{eX} + 3(\epsilon_{\alpha\beta}^{uX} + \epsilon_{\alpha\beta}^{dX}) \tag{4.10}$$

Now, $\epsilon_{\alpha\beta}$ enters the Hamiltonian as entries of a potential-like matrix. In Eq. 4.11, $A_{CC}\text{diag}(1, 0, 0)$ is our familiar matter potential from the Standard Model. There is also our new term, $A_{CC}\epsilon$, which contains

[4] The extreme lightness might be explained by a mass generation at a higher order theory.

the components $\epsilon_{\alpha\beta}$:

$$\begin{aligned} H &= \frac{1}{2E}\left[UM^2U^\dagger + A_{CC}\,\mathrm{diag}(1,0,0) + A_{CC}\,\epsilon\right] \\ &= \frac{1}{2E}\left[UM^2U^\dagger + A_{CC}\begin{pmatrix} 1+\epsilon_{ee} & \epsilon_{e\mu} & \epsilon_{e\tau} \\ \epsilon_{\mu e} & \epsilon_{\mu\mu} & \epsilon_{\mu\tau} \\ \epsilon_{\tau e} & \epsilon_{\tau\mu} & \epsilon_{\tau\tau}\end{pmatrix}\right]. \end{aligned} \tag{4.11}$$

In the limit $\epsilon_{\alpha\beta} \to 0$, we recover the standard interaction Hamiltonian from Eq. 2.56. We can draw several conclusions from this form of the Hamiltonian. Any nonzero off-diagonal element $\epsilon_{\alpha\beta}, \alpha \neq \beta$ will make the NSI violate lepton flavor, just as the off-diagonal elements of U does in the SM. Moreover, since the SM potential has the same order in A_{CC} as the NSIs, any $\epsilon_{\alpha\beta} \sim 1$ will make the new matter effect be the same order as the SM effect.

We have two more modifications to the matrix ϵ. First, all terms of the Hamiltonian must of course be Hermitian, thus

$$\begin{pmatrix} \epsilon_{ee} & \epsilon_{e\mu} & \epsilon_{e\tau} \\ \epsilon_{\mu e} & \epsilon_{\mu\mu} & \epsilon_{\mu\tau} \\ \epsilon_{\tau e} & \epsilon_{\tau\mu} & \epsilon_{\tau\tau}\end{pmatrix} = \begin{pmatrix} \epsilon_{ee} & \epsilon_{e\mu} & \epsilon_{e\tau} \\ \epsilon_{e\mu} & \epsilon_{\mu\mu} & \epsilon_{\mu\tau} \\ \epsilon_{e\tau} & \epsilon_{\mu\tau} & \epsilon_{\tau\tau}\end{pmatrix}. \tag{4.12}$$

Now we have reduced the possible number of NSI parameters from 9 down to 6.

By combining oscillation data and neutrino-nucleon scattering at the COHERENT experiment, 90 % CL ranges of some of the NSI parameters were constrained in [25] to

$$\begin{aligned} -0.090 <& \epsilon_{\tau\tau} < 0.38 \\ -0.01 <& \epsilon_{\mu\tau} < 0.009 \\ -0.073 <& \epsilon_{e\mu} < 0.044 \\ -0.15 <& \epsilon_{e\tau} < 0.13\,. \end{aligned} \tag{4.13}$$

4.2.2 IceCube Signal

In our analysis of IceCube, we are constrained to muon track events. Thus, we are not able to test any theory which does not modify $P_{\alpha\mu}$. Moreover, the IceCube data is avaibable in the range 500 GeV to 10 TeV range, where any rapid oscillations have settled down.

Since all standard matter potentials are diagonal, the elements $\epsilon_{\alpha\beta}$, $\alpha = \beta$ will directly adjust the matter potential felt by flavor α. The off-diagonal terms have a more interesting theoretical implication as they open up matter interactions across flavors. Remember, in the Standard model, we are restriced to weak interactions that conserve lepton number. However, a off-diagonal NSI parameter allows flavor transitions during matter interactions. Thus, the off-diagonal elements constitute new soures of flavor violation. Moreover, $\epsilon_{\alpha\beta}$ modifies the $\nu_\alpha \to \nu_\beta$ transition independently of the mixing matrix. Thus, we can in theory boost a flavor transition which is supressed by the mixing matrix. Moreover, since we have 6 NSI parameters, and the PMNS matrix is parametrized with only 3 parameters, we have more degrees of freedom when adjusting the probabilities using the NSI matrix. Each term in the PMNS matrix consists of at least two of the three mixing angles, making them much more dependent on each other.

As discussed in Eq. 2.15, the atmospheric $\nu_\mu \to \nu_\tau$ transition will be the most abundant, making $\epsilon_{\mu\tau}$, $\epsilon_{\mu\mu}$, $\epsilon_{\tau\tau}$ the most suitable NSI parameters to constrain from muon events. As we will see, $\epsilon_{e\mu}$ is also a candidate, alebit a weaker one.

In Fig. 4.2, we see how the introduction of $\epsilon_{\mu\tau} = 0.02$ alters the ν_μ and $\bar{\nu}_\mu$ survival probabilities for neutrinos that traverse the entire Earth diameter (i.e. $\cos(\theta_z^{true}) = -1$). $\epsilon_{\mu\tau}$ does not dramatically change neither amplitude nor frequency of the probabilities. Instead, it seems to strech or compress the oscillations. Since the only difference between the way neutrinos and antineutrinos interact with matter is the sign of the potential, the probability for ν_μ with positive $\epsilon_{\alpha\beta}$ is identical to the probability for $\bar{\nu}_\mu$ with negative $\epsilon_{\alpha\beta}$. Thus, the dashed line in the right panel not only shows the survival probability for $\bar{\nu}_\mu$ with $\epsilon_{\mu\tau} = 0.02$, but also the survival probability for ν_μ with $\epsilon_{\mu\tau} = -0.02$. Hence, we note that $\epsilon_{\mu\tau} > 0$ stretches (compresses) $P_{\mu\mu}$ for neutrinos (antineutrinos), while $\epsilon_{\mu\tau} < 0$ compresses (stretches) $P_{\mu\mu}$ for neutrinos (antineutrinos).

The value of $\epsilon_{\tau\tau}$ does not affect neither $P_{\mu\mu}$ nor $P_{\bar{\mu}\bar{\mu}}$, in the IceCube region above 500 GeV. Hence, we will not be able to say anything about $\epsilon_{\tau\tau}$ in our IceCube study. Comparing the probabilities in

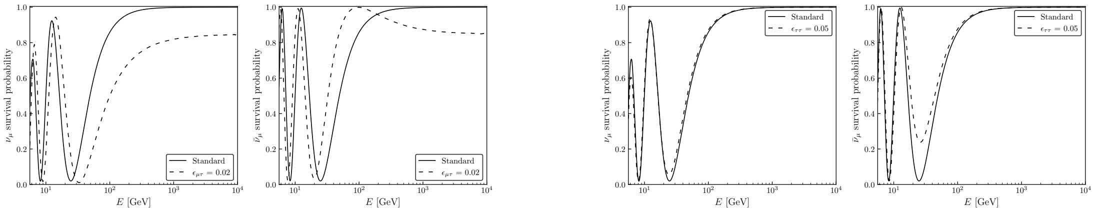

Figure 4.2: *Left panel:* Muon neutrino and antineutrino survival probabilities for $\cos(\theta_z^{true}) = -1$ when $\epsilon_{\mu\tau} = 0.02$. All other NSI parameters are fixed to zero. *Right panel:* Muon neutrino and antineutrino survival probabilities for $\cos(\theta_z^{true}) = -1$ when $\epsilon_{\tau\tau} = 0.05$. All other NSI parameters are fixed to zero.

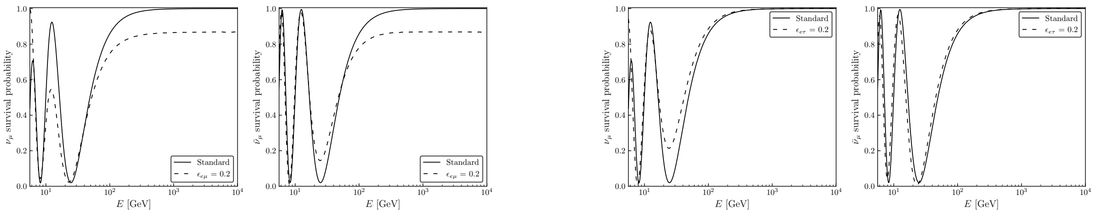

Figure 4.3: Muon neutrino and antineutrino survival probabilities for $\cos(\theta_z^{true}) = -1$*Left panel:* $\epsilon_{e\mu} = 0.2$. All other NSI parameters are fixed to zero. *Right panel:* $\epsilon_{e\tau} = 0.2$. All other NSI parameters are fixed to zero.

Fig. 4.2 with $\epsilon_{\tau\tau} = 0.05$ with the ones for $\epsilon_{\mu\tau} = 0.02$ in Fig. 4.2, we see that even though we let $\epsilon_{\tau\tau}$ take 2.5 times the value of $\epsilon_{\mu\tau}$, its effect on $P_{\mu\mu}$ is smaller. The weakening of the $P_{\bar{\mu}\bar{\mu}}$ resonance will be visible in DeepCore, but we should expect a less stringent constraint due to the weakness of the effect compared to $\epsilon_{\mu\tau}$.

Thus, we will use IceCube to constrain $\epsilon_{\mu\tau}$ only.

Moving on to $\epsilon_{e\mu}$ and Fig. 4.3, we see that both probabilities has shifted downwards for $E^{true} > 500$ GeV. In Fig. 4.3, we see that the muon channel remains largely unaffected of the value of $\epsilon_{e\tau}$ as we expected. The expection of this lies in the DeepCore region of rapid oscillations, where mixing is more violent.

4.2.3 DeepCore and PINGU Signals

Now we repeat our proability analysis but for the DeepCore/PINGU region of 5.6 GeV to 56 GeV. As we previously saw, we have rapid oscillations, which means that 'indirect' modifications (i.e. $\epsilon_{e\tau}$ will affect the $P_{\mu\mu}$ channel) will be more apparent, since all flavors are involved to a greater degree compared with the more stable region above 500 GeV, where many oscillations have settled down.

Another feature of our DeepCore study includes the fact that we now have access to cascade events, in which ν_e and ν_τ are more abundant. Thus, we are no longer constrained to the μ channel alone, but we can now find interesting features in the other channels too. However, we remember that the ν_μ flux is still the most abundant.

Fig. 4.2 shows that $\epsilon_{\mu\tau}$ affects both $P_{\mu\mu}$ and $P_{\bar{\mu}\bar{\mu}}$ over the whole energy range. Since IceCube also sees this, we hope to be able to boost the constraining of $\epsilon_{\mu\tau}$ by combining the two experiments.

Regarding $\epsilon_{\tau\tau}$ in Fig. 4.3, the signal mainly shows in the $P_{\bar{\mu}\bar{\mu}}$ channel as a weaker resonance dip in the 20 GeV region. Thus, DeepCore/PINGU alone will be used to constrain this parameter.

$\epsilon_{e\mu}$ in Fig. 4.3 shows weak resonance dampening for both ν_μ and $\bar{\nu}_\mu$.

For $\epsilon_{e\tau}$, we see a similar resonance dampening in $P_{\mu\mu}$ as we did with $\epsilon_{\tau\tau}$ for $P_{\bar{\mu}\bar{\mu}}$. Hence, we should be able to see the $\epsilon_{e\tau}$ effect in DeepCore/PINGU, but remember that we now have the option to look at the other flavor channels.

Fig. 4.4 shows the electron neutrino and antineutrino survival probabilities, and here we see a clear difference when turning on $\epsilon_{e\tau}$.

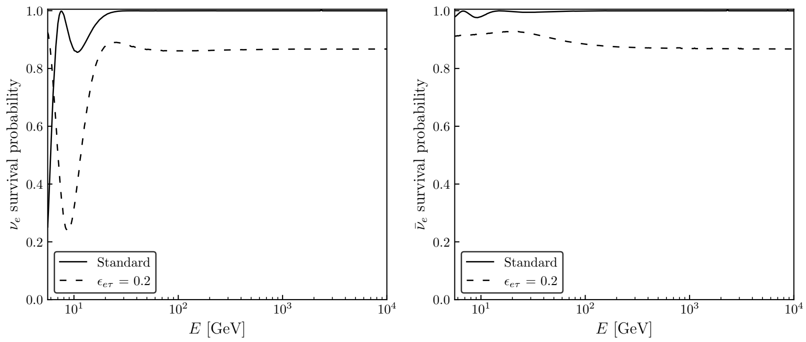

Figure 4.4: Electron neutrino and antineutrino survival probabilities for $\cos(\theta_z^{true}) = -1$ when $\epsilon_{e\tau} = 0.2$. All other NSI parameters are fixed to zero.

We plot the event pull $(N_{NSI} - N_{SI})/\sqrt{N_{SI}}$ where $N_{(N)SI}$ are the numbers of expected events assuming (non-)standard interactions in Fig. 4.5. This gives the normalized difference in the number of expected events at the detector, and illustrates the expected sensitivity of DeepCore for the NSI parameters.

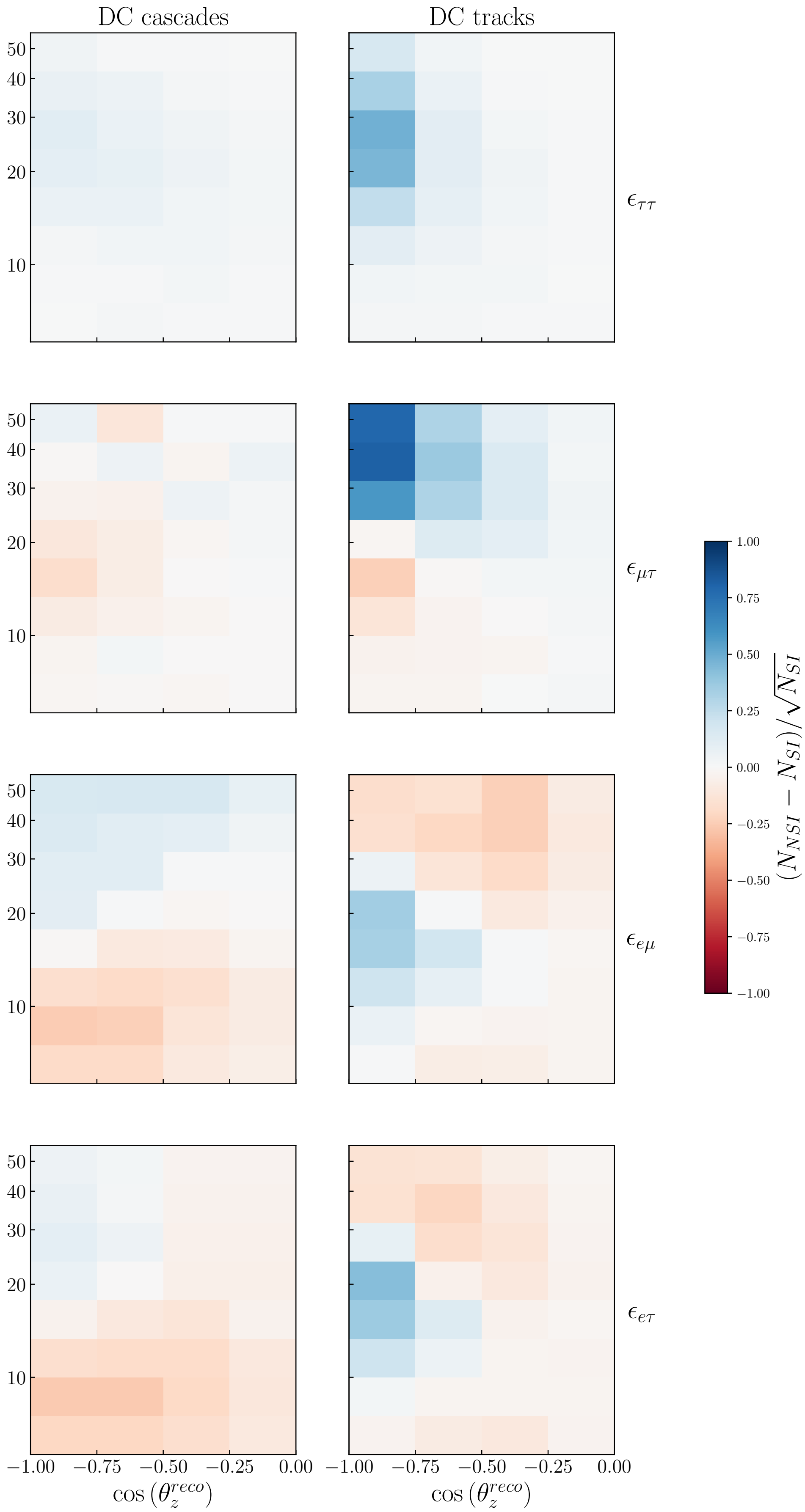

Figure 4.5: Plots of the quantity $(N_{NSI} - N_{SI})/\sqrt{N_{SI}}$, displaying which reconstructed bins the NSI signal is most clear.

Chapter 5

Results

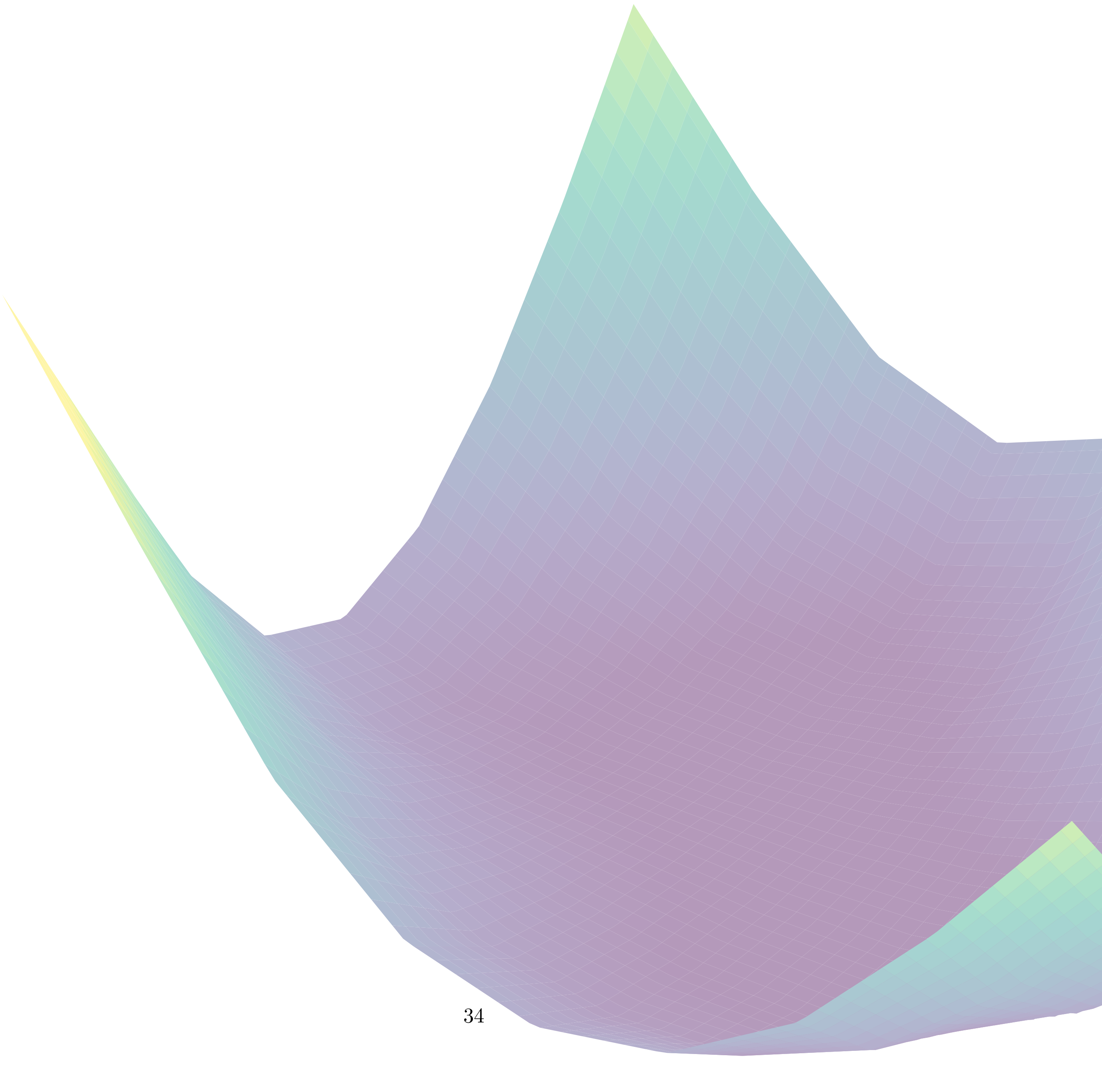

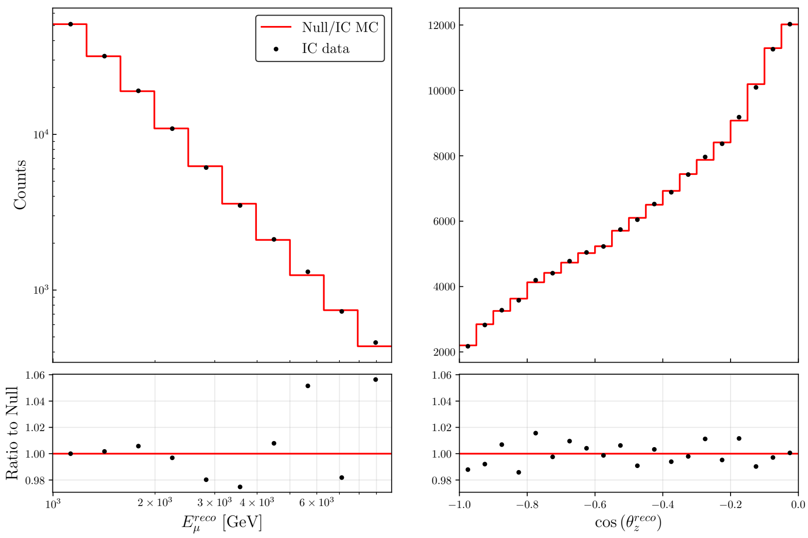

Figure 5.1

5.1 The Sterile Hypothesis

With the null (3ν) hypothesis normalized to the IceCube Monte Carlo as in Eq. 3.5, we are now in good shape to study the sterile effect on the probabilities, and how that compares to data. First, let us see how the collected data from Fig. 3.5 deviates from the predicted 3ν oscillations. Fig. 5.1 shows an impressive agreement to the standard 3ν oscillation picture, with the largest deviations of 6% for neutrinos close to double-digit TeV values. In zenith, the data only deviates $\pm 1\%$. Recalling the TeV disappearance from Fig. 4.1a, we see that we have a similar deficiency found in the data at 4 TeV. Thus, we expect the best fitting sterile hypothesis to include a Δm_{41}^2 that places the resonant disappearance in the same region. From Fig. 4.1b, we see that a mass of $\Delta m_{41}^2 = 1.5\,\mathrm{eV}^2$ achieves this.

5.1.1 χ^2 Minimization

For our analyses, we define our χ^2 as

$$\chi^2(\hat{\theta}, \alpha, \beta) = \sum_{ij} \frac{\left(N^{\rm th} - N^{\rm data}\right)_{ij}^2}{\left(\sigma_{ij}^{\rm data}\right)^2 + \left(\sigma_{ij}^{\rm syst}\right)^2} + \frac{(1-\alpha)^2}{\sigma_\alpha^2} + \frac{\beta^2}{\sigma_\beta^2} \tag{5.1}$$

where we minimize over the model parameters $\hat{\theta}$, the penalty terms α and β. $N_{ij}^{\rm th}$ is the expected number of events from theory, and $N_{ij}^{\rm data}$ is the observed number of events in that bin. We set $\sigma_\alpha = 0.25$ as the atmospheric flux normalization error, and $\sigma_\beta = 0.04$ as the zenith angle slope error [9]. The observed event number has an associated Poissonian uncertainty $\sigma_{ij}^{\rm data} = \sqrt{N_{ij}^{\rm data}}$. For IceCube, the event count takes the form

$$N_{ij}^{\rm th} = \alpha\left[1 + \beta(0.5 + \cos{(\theta_z^{reco})_i})\right] N_{ij}(\hat{\theta})\,, \tag{5.2}$$

with $N_{ij}(\hat{\theta})$ from Eq. 3.5. Here, the term $\beta(0.5+\cos{(\theta_z^{reco})_i})$ allows the event distribution to rotate with angle β around the median zenith angle of $\cos{(\theta_z^{reco})} = -0.5$. We also have an uncorrelated systematic error $\sigma_{ijk}^{\rm syst}$. We set $\sigma_{ijk}^{\rm syst} = f\sqrt{N_{ijk}^{\rm data}}$, where f is a percentage of our own choosing.

The minimization of Eq. 5.1 simply returns a value for each set of model parameters. We use this value to quantify to what extent our theoretical simulations $N_{ij}^{\rm th}$ agree with the data $N_{ij}^{\rm data}$ within the error bounds provided by σ_a, σ_b, and f. We then select the set of χ^2 values which are the smallest and our allowed parameters are then their associated $\hat{\theta}$. We then translate the χ^2 distribution by subtracting the best-fit point, and analyze $\Delta\chi^2 = \chi^2 - \chi^2_{min}$. From the χ^2-distribution, one can show that the 90%

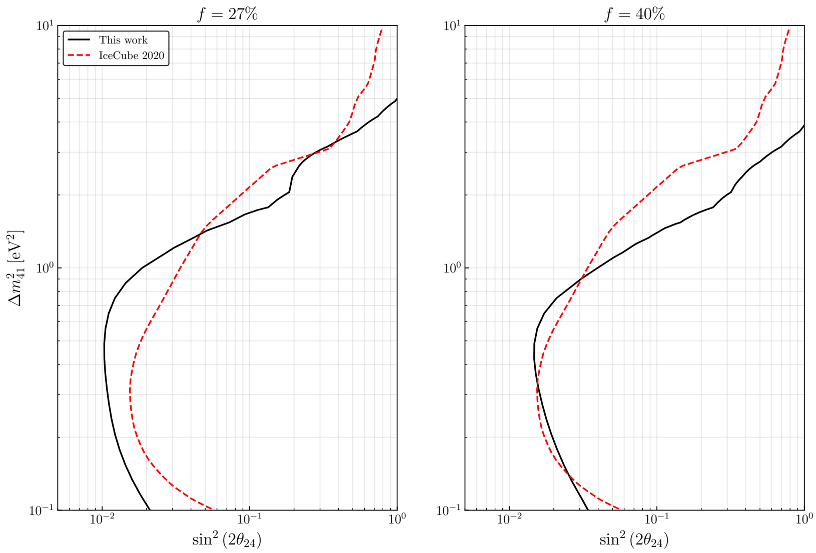

Figure 5.2: The 90% CL contour with two different systematic error scalings, compared with the official IceCube result from [12]

confidence level has a value of 2.71 for two degrees of freedom. When slicing through the two-dimensional grid of $\Delta\chi^2$ at this level, we then obtain a contour plot that tells us what regions are within our 90% and what regions are not.

5.1.2 Sterile Mass and Mixing

Let us start with looking at the best-fit event distribution resulting from the χ^2 minimization. Fig. 5.4 now contains the best-fit event distribution assuming the sterile hypothesis. The best-fit values are $\Delta m^2_{41} = 0.01\,\mathrm{eV}^2$ and $\sin(2\theta_{24})^2 = 0.67$ ($\theta_{24} = 27.5°$). The contour plot shown in Fig. 5.3 divides the parameter space into two regions. To the right of the boundary, the $\Delta\chi^2$ has values above the confidence level, meaning that those parameter pairs can be excluded at a certain confidence level.

By tuning the scaling f of the uncorrelated systematic error, we can shift the contour. We extract the contour from the IceCube sterile analysis [12], and compare in Fig. 5.2. We see that the contour in the higher Δm^2_{41} region above $1\,\mathrm{eV}^2$ is very sensetive to the tuning, while the lower region between $1 \times 10^{-1}\,\mathrm{eV}^2$ to $1\,\mathrm{eV}^2$ remains fixed. We put $f = 35\%$ and compare our results to the Giunti et al. [26] in Fig. 5.3. Here, we see that our lower fixed region between $1 \times 10^{-1}\,\mathrm{eV}^2$ to $1\,\mathrm{eV}^2$ is closer to the IceCube result than Giunti et al, but that our contour slightly diverges above $1\,\mathrm{eV}^2$.

We now in Fig. 5.4 plot the best-fit sterile hypothesis with the data from Fig. 5.1, to finally see how the best sterile hypothesis compares to data.

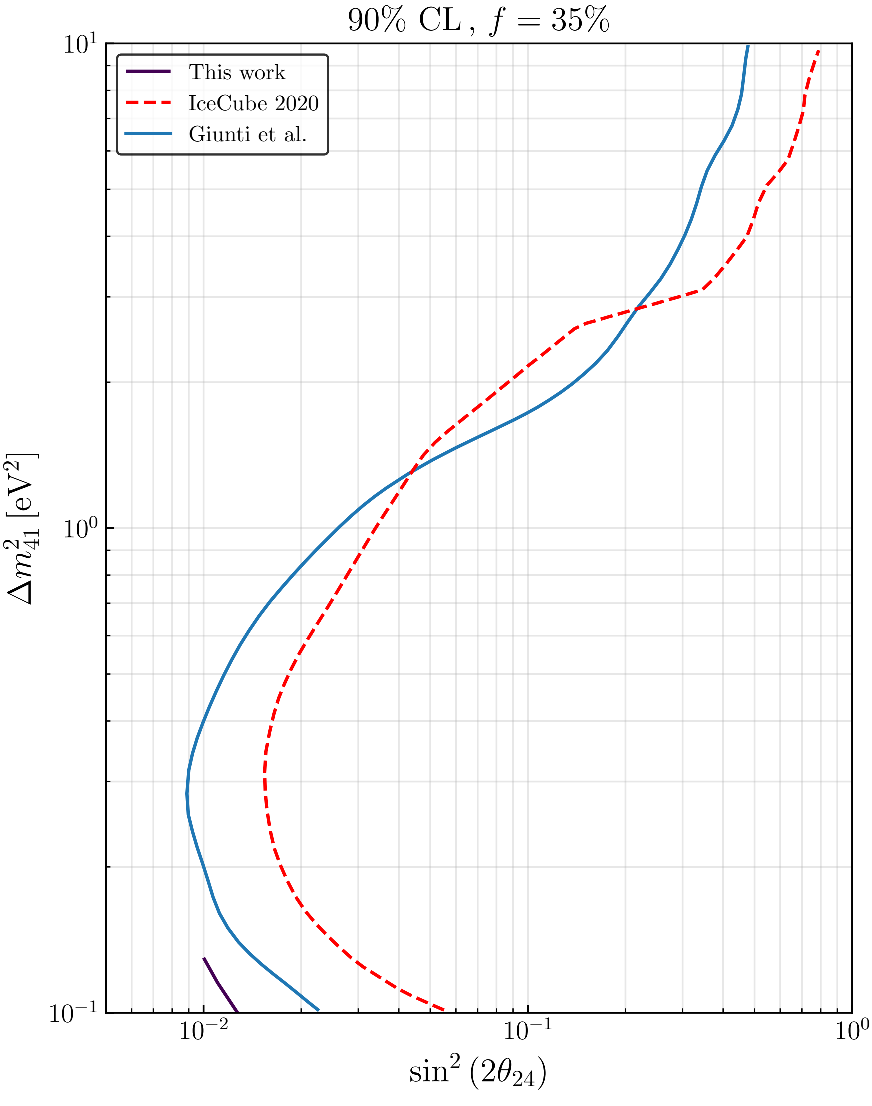

Figure 5.3: The 90% CL contour using $f = 35\%$, compared with the official IceCube result from [12] and the result from [26]

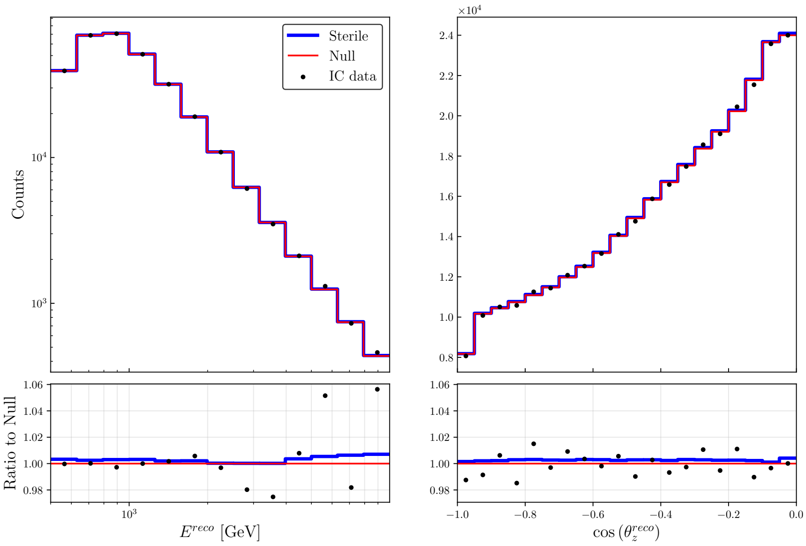

Figure 5.4: The predicted binned event count assuming our best-fit sterile hypothesis, compared with the null and data.

5.2 Non-Standard Interactions

5.2.1 χ^2 Minimization

The χ^2 takes the same form as in Eq. 5.1, namely

$$\chi^2(\hat{\theta}, \alpha, \beta) = \sum_{ij} \frac{\left(N^{\text{th}} - N^{\text{data}}\right)^2_{ij}}{\left(\sigma^{\text{data}}_{ij}\right)^2 + \left(\sigma^{\text{syst}}_{ij}\right)^2} + \frac{(1-\alpha)^2}{\sigma^2_\alpha} + \frac{\beta^2}{\sigma^2_\beta} \tag{5.3}$$

Just as with the sterile analysis, the IceCube event count takes the form

$$N^{\text{th}}_{ij} = \alpha \left[1 + \beta(0.5 + \cos{(\theta^{reco}_z)}_i)\right] N_{ij}(\hat{\theta}) \,. \tag{5.4}$$

For DeepCore and PINGU however, the event count takes the form

$$N^{\text{th}}_{ijk} = \alpha \left[1 + \beta \cos{(\theta^{reco}_z)}_i\right] N_{ijk}(\hat{\theta}) + \kappa N^{\mu_{atm}}_{ijk} \,, \tag{5.5}$$

with $N_{ijk}(\hat{\theta})$ from Eq. 3.6. $N^{\mu_{atm}}_{ijk}$ is the muon background, which is left to float freely in the DeepCore analysis. The background at PINGU can be considered neglible to first order [16], and we thus put $\kappa = 0$ when calculating the PINGU χ^2. For IceCube, we set $\sigma^{\text{syst}}_{ijk} = f\sqrt{N^{\text{data}}_{ijk}}$. For DeepCore, we use the provided systematic error distribution which accounts for both uncertanties in the finite MC statistics and in the data-driven muon background estimate [13].

5.2.2 Constraining Parameters